




SAFIR 2010 FRAS

Numerical Studies on Dynamic Behaviour of Pipelines, Part 2

Authors: Kim Calonius

Confidentiality: Public

| | | |
|--|---|---|
| Report's title Numerical Studies on Dynamic Behaviour of Pipelines, Part 2 | | |
| Customer, contact person, address SAFIR 2010 VYR | Order reference | |
| Project name Fracture assessment for reactor circuit (FRAS) / Loads transferred by supports | Project number/Short name 13511-FRAS | |
| Author(s) Kim Calonius | Pages 46/ - | |
| Keywords Loads, supports, pipe break, FEM, reactor circuit | Report identification code VTT-R-01214-10 | |
| <p>Summary</p> <p>Dynamic excitation due to a pipe break can cause pipe to abruptly displace and hit the components, instrumentation and equipment nearby. In order to minimize the extensive damage caused by such pipe whips in a nuclear power plant, different types of restraints and supports are designed for the pipelines.</p> <p>Here, the usability of different types of elements provided by Abaqus, a commercial general-purpose finite element code, in modelling the dynamic behaviour of pipelines is tested. A relatively short pipe line section with one bend and one restraint is chosen as a test case. Simple and typical nuclear power plant pipeline geometry and materials are chosen. The chosen basic elbow element model is based on the previous studies within the same project, where it was found adequate. Some parameters and properties are improved from the previous studies. Some sensitivity study is conducted.</p> <p>The post-yield behaviour of the pipe steel material has some notable effect on the behaviour of the pipe in a guillotine pipe break. The maximum forces were of slightly different, but in every case with otherwise same parameters a plastic hinge was formed at the restraint and the analysis terminated. Obviously, rate dependence makes the structure slightly dynamically stiffer.</p> <p>The inner pressure of the pipe and its assumed decay after the pipe break has a major influence on the results. If the pressure rapidly decays instead of being constant, the pipe still hits the restraint, but the force is less than half and no plastic hinge is formed.</p> <p>By comparing the results with different types of spring behaviours and a detailed finite element modelling of the pipe and restraint, it was seen, that the spring element should include the gap and some softening, i.e. curvature in the stiffness curve, but not necessarily directly the stress-strain curve of the material.</p> <p>The mass of the water has only minor effect on the dynamic behaviour of the pipe in this kind of highly dynamic loading.</p> <p>Earthquake simulation was briefly studied with the same model. The nonlinear dynamic analyses were conducted according to the Eurocodes.</p> | | |
| Confidentiality | Public | |
| Espoo 26.4.2010 | | |
| Signatures  | Signatures  | Signatures  |
| Written by Kim Calonius, Research Scientist | Reviewed by Otso Cronvall, Research Scientist | Accepted by Eila Lehmus, Technology Manager |
| VTT's contact address P.O.Box 1000, 02044 VTT | | |
| Distribution (customer and VTT) SAFIR2010 Reference Group 6, VTT SAFIR2010 FRAS Ad Hoc Group | | |
| <p><i>The use of the name of the VTT Technical Research Centre of Finland (VTT) in advertising or publication in part of this report is only permissible with written authorisation from the VTT Technical Research Centre of Finland.</i></p> | | |

Preface

This report has been prepared under the research project FRAS 1.1; “Loads Transferred by Supports”, which concerns external loads transferred to the reactor circuit components by different types of supports. The project is a part of SAFIR2010 - The Finnish Research Programme on Nuclear Power Plant Safety (2007 – 2010). FRAS 1.1 project work in 2009 was funded by the State Nuclear Waste Management Fund (VYR) and the Technical Research Centre of Finland (VTT). The work was carried out at VTT. The author of the report expresses his gratitude Otso Cronvall (VTT) for reviewing this report and to Päivi Karjalainen-Roikonen (VTT) for managing FRAS project.

Espoo 26.4.2010

Author

Contents

| | |
|---|----|
| Preface | 2 |
| 1 Introduction..... | 4 |
| 2 New features in finite element modelling of pipelines | 5 |
| 3 Model descriptions..... | 7 |
| 3.1 Geometry | 7 |
| 3.2 Finite element mesh..... | 8 |
| 3.3 Materials | 10 |
| 3.4 Boundary conditions | 11 |
| 3.5 Inner pressure..... | 13 |
| 4 Dynamic analysis of a guillotine pipe break with old parameters..... | 14 |
| 5 Dynamic analysis of a guillotine pipe break with new parameters | 23 |
| 6 Dynamic analysis of an earthquake with new parameters | 35 |
| 7 Conclusions and future work | 45 |
| References | 46 |

1 Introduction

Every continuum structure can be modelled and solved numerically with general-purpose solid continuum volume elements. However, that can be very ineffective and time-consuming, since usually a very large number of volume elements is needed to capture the right behaviour. That is why it is useful to have structural and special-purpose elements instead.

The pipes in power plants are long, slender structures with relatively thin walls. Therefore, it is convenient to model them with shell elements. Since the beam theory can be used to calculate their behaviour quite accurately, also pipe elements can be used. Beam, elbow, shell and solid volume elements are used in this study for modelling the pipe.

There are many types of structural supports and restraints in power plants. They support components and pipelines mainly against the gravitational forces acting in vertical direction. Either the components rest on the supports or they are suspended by the so-called hangers. The function of restraints is to take the dynamic loads in case of accidents such as pipe breaks or earthquakes when the pipes can have exceptionally large movements and velocities. The thermal expansion is taken into account by leaving sufficiently large gaps between the pipes and restraints.

The essential difference between the pipe break and earthquake is that in the former case the force actuates from within the power plant component and is transferred by different types of supports to the surrounding structures while in the latter case it is vice versa.

If special-purpose elements are not used, contact behaviour has to be formulated between the pipe and restraint surfaces. That is also why it is useful to have special-purpose elements instead, which can include the gap, contact, stiffness and even possible viscous properties. Solid volume, spring elements and pipe support elements are used in this study for modelling the restraint.

This study concentrates on simulating the dynamic behaviour of a relatively short pipe section with one restraint. Previously, its stiffness was first calculated with a relatively detailed finite element model (reported in Calonius, 2008), which was then substituted with a simpler model using structural and special purpose elements (Calonius, 2008 and 2009). A pipe guillotine break has previously been chosen as a dynamic test case and it has been simulated with different kinds of models. A model with elbow elements was then discovered to be adequate. The main aim here is not to simulate the pipe break as realistically as possible, but to compare different model and analysis types with each other.

In this report, in addition to the old model, a new model with a slightly modified geometry was used. In case of both models, a sensitivity study was conducted by varying some properties and characteristics. Earthquake is also briefly considered with the new geometry.

To begin with, new features in latest Abaqus versions that could be useful in this field of study are considered.

2 New features in finite element modelling of pipelines

New features in latest Abaqus versions that could be useful in this field of study are considered in this chapter. Although mainly the newest version was used in this study, these features were not yet utilized. Most of them would have been useful. The features mentioned below are gathered from the newest online Abaqus manual (Abaqus, 2009).

Version 6.7

There are some enhancements to analytical fields in Abaqus/CAE. You can now use analytical fields to define spatially varying loads over a region for additional loads and boundary conditions.

The fully integrated shell element S4, solid elements C3D8 and C3D8I, and thermally coupled solid element C3D8T previously available in Abaqus/Standard are now available in Abaqus/Explicit.

The part and assembly display options now include a Render beam profiles option. This option allows you to view an idealized representation of the shape-based or generalized beam profile that you assigned to a wire part. You can also view the profile of a truss.

Version 6.8

The output database display options now include a Render beam profiles option. This option enables you to view an idealized representation of the shape-based or generalized profile associated with a beam element. You can also view the profile of a truss element. The Render beam profiles option was previously available only in the part and assembly display options.

Some more enhancements to analytical fields in Abaqus/CAE have been introduced. You can use analytical fields to define spatially varying parameters over a region for the following additional interactions and prescribed conditions:

- Interactions: Concentrated radiation to ambient and surface radiation to ambient
- Loads: Body charge, body current, body force, concentrated charge, concentrated concentration flux, concentrated current, concentrated force, concentrated heat flux, moment, concentrated pore fluid, Coriolis force, generalized plane strain, gravity, inward volume acceleration, line load, rotational body force, surface charge, and surface current
- Boundary conditions: Acceleration/angular acceleration and velocity/angular velocity.
- Predefined fields: Velocity

Version 6.8 has enhanced Eulerian capabilities in Abaqus/Explicit. In the traditional Lagrangian finite element formulation elements are always 100% full of material, and the deformation of the material is determined by the deformation of the element mesh. In the Eulerian formulation the element mesh is rigidly fixed in space for the duration of the analysis; however, material can flow across element boundaries, and elements are not always

100% full of material. Because the mesh is rigid, the Eulerian technique avoids the difficulties associated with element distortion in extreme deformations.

The finite-sliding, surface-to-surface contact formulation in Abaqus/Standard no longer restricts the number of surface faces that can share a common node in two dimensions or a common edge in three dimensions. Surfaces with T-intersections and other complex intersections, which are common in shell models, can act as a slave or master surface with this formulation in Abaqus/Standard.

Contact output in Abaqus/Standard has been enhanced to provide contact stress output on both surfaces of two-surface contact pairs. In previous releases of Abaqus/Standard this output was provided only on slave surfaces of contact pairs. In addition, Abaqus/Standard can provide output of contact nodal force vectors and nodal areas associated with active contact constraints. These changes apply to output to the output database (.odb) file but not to the data (.dat) and results (.fil) files. Output of contact stresses and contact nodal forces for all contact surfaces was available in previous releases of Abaqus, but only for Abaqus/Explicit analyses.

Version 6.9

Exchanging Abaqus/CAE data with Microsoft Excel is now supported. The Excel Utilities plug-in enables you to exchange amplitude data and X–Y data between Abaqus/CAE and Excel.

The material orientations options have been enhanced. A new Orientations container is now in the Model Tree under the part. To edit, suppress, or resume a material orientation, click mouse button 3 on the material orientation in the Model Tree and select from the list that appears.

Abaqus/Standard to Abaqus/Explicit co-simulation is now supported. Abaqus/Standard and Abaqus/Explicit each have unique simulation strengths. For example, Abaqus/Standard provides a very general substructuring capability that enables cost-effective analysis of bodies subjected to small strains, while Abaqus/Explicit excels at simulating high-speed events. Abaqus/Standard to Abaqus/Explicit co-simulation provides you with a general tool to combine the strengths of each analysis program to more effectively perform complex simulations.

A general contact capability is now provided in Abaqus/Standard with nearly the same user interface as the pre-existing general contact capability in Abaqus/Explicit. The general contact algorithm is intended to eventually become the primary contact algorithm, but more robust and economical solutions in Abaqus/Standard can often be obtained with traditional contact pair definitions as compared to highly automated general contact definitions in this initial release of general contact. Some users may prefer to wait for the general contact implementation in Abaqus/Standard to further mature; however, many users will benefit from this initial release of general contact in terms of the simplicity of defining contact and the accuracy of solutions obtained with it.

3 Model descriptions

Since a sensitivity study is conducted and adequacy of different model types is assessed, it is practical that the structure itself is not too complex with many variables. A relatively short pipe section with one restraint and one bend is studied. The whole combined model consists of three parts: the pipe, a steel restraint with a small gap (6 cm in size), and a concrete block which represents surrounding structures such as part of containment wall near the pipeline.

The model is the same as used in previous studies (Calonius, 2008) and (Calonius, 2009), but with slight modifications. The finite element meshes and element types (elbow and shell) are the same as used in the final main models of previous study (Calonius, 2009). Two slightly different geometries are used. The old cross-sectional dimensions are modified for the new geometry.

3.1 Geometry

Figure 1 shows the old example pipeline geometry simulated in this study together with main dimensions. The lower right end of the pipe is rigidly fixed and the postulated pipe break takes place in the upper left end of the section. Some of the old dimensions are confidential and not shown in this report.

Figure 2 shows the new example pipeline geometry simulated in this study together with main dimensions.

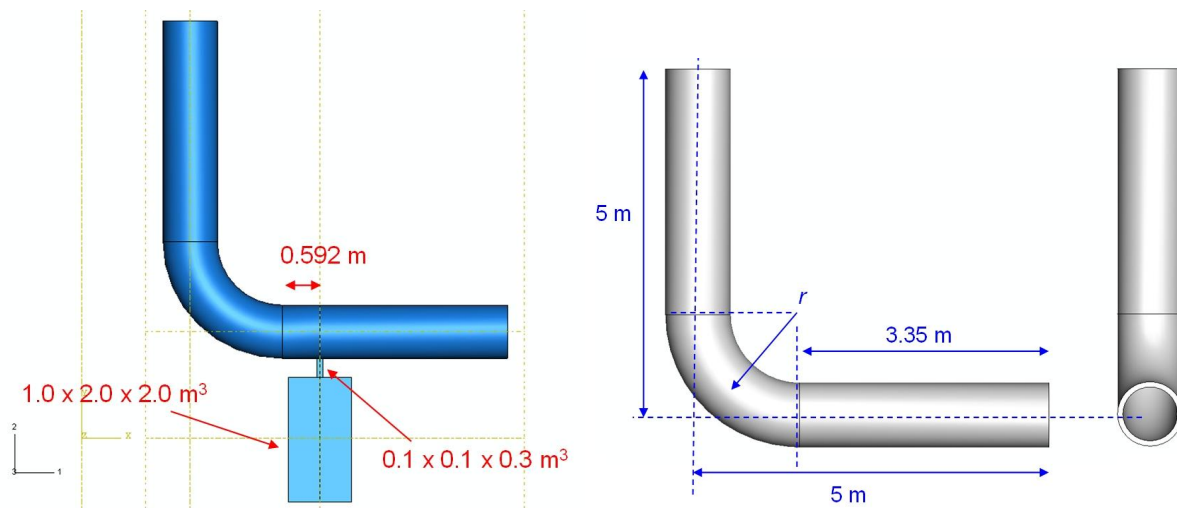


Figure 1. Old dimensions of the pipeline section.

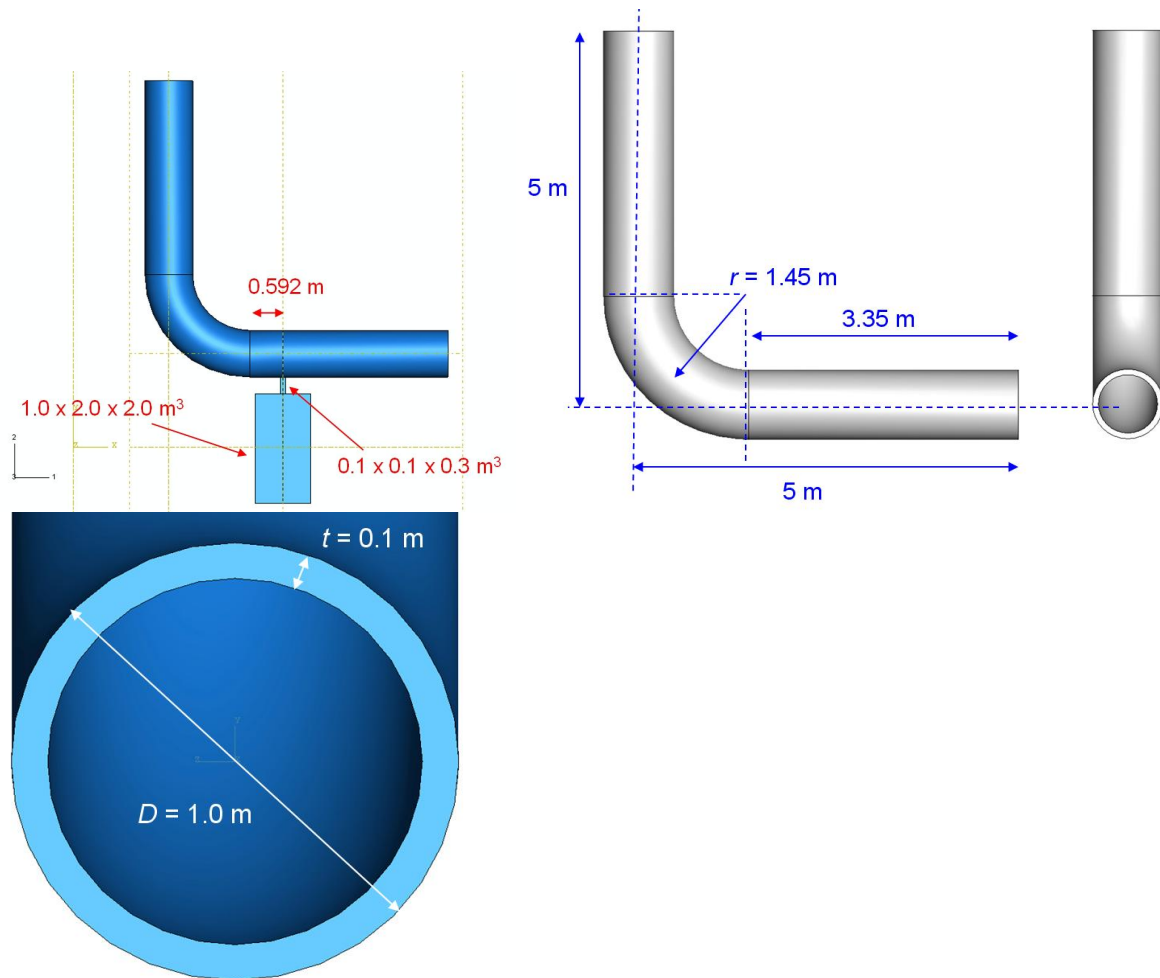


Figure 2. New dimensions of the pipeline section.

3.2 Finite element mesh

The different finite element model types are shown in Figure 3. The concrete block and the restraint are modelled either with solid volume elements (referred to as C3D8R in Abaqus) or with a spring element (SPRINGA). The pipe is modelled with shell or elbow elements. The elbow model has altogether 18 (ELBOW31) elements (6 elements along the bend). The spring element representing the restraint can also be seen near the bend in the horizontal section.

The shell element model has 44 shell elements (S4R) around the pipe circumference and the total number of elements is 6 864.

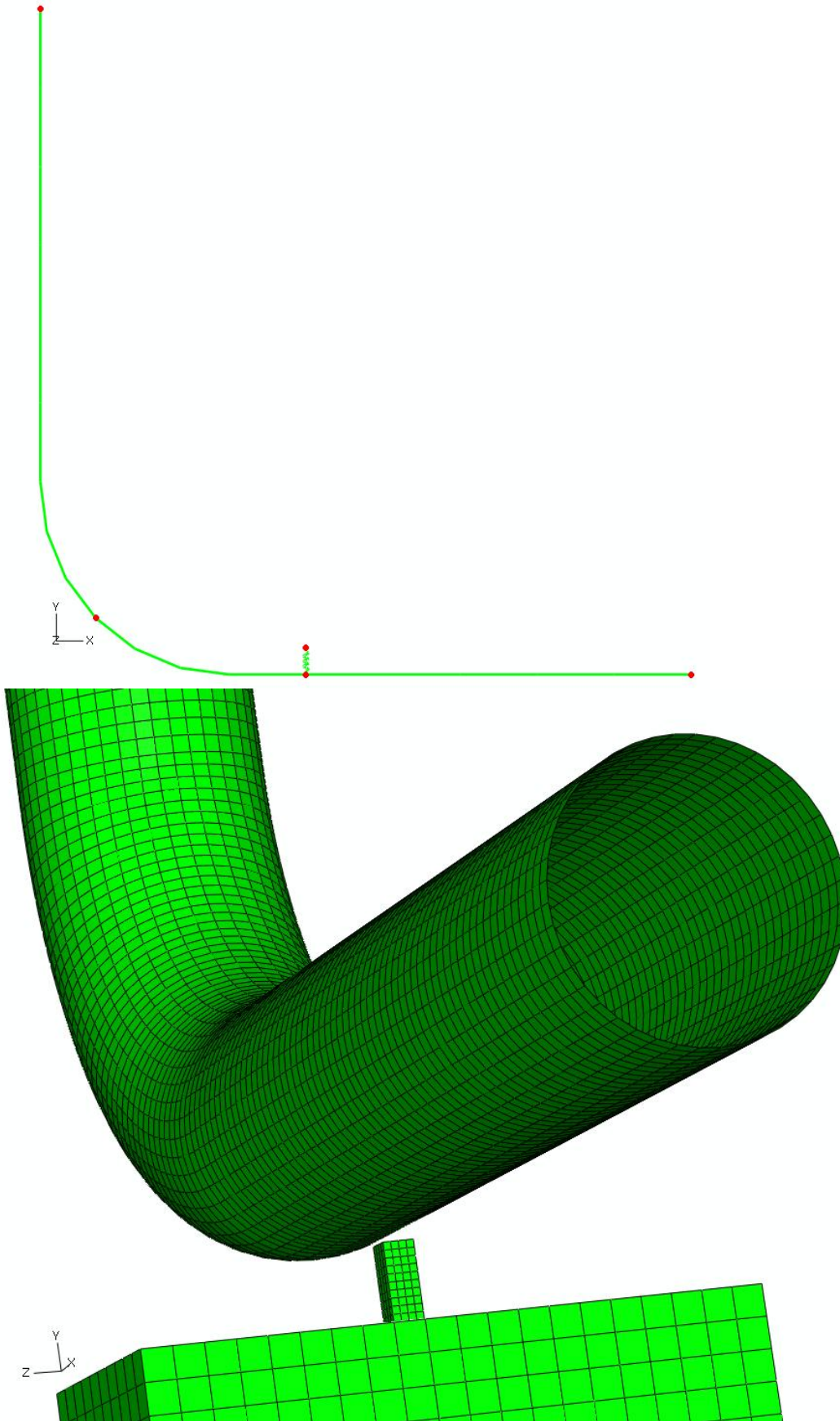


Figure 3. Elbow (above) and shell (below) element meshes. The restraint is modelled either with a spring element (above) or with solid elements (below).

3.3 Materials

Four materials are used - three steel material types and one concrete material type. Depending on the analysis in question, the pipe is assigned either material A, B or C. The simple steel rod of the restraint with a square cross-section is always assigned steel type B. Water is not included, but its mass is taken into account in one of the analyses. The high inner pressure is applied in every analysis. The linear material properties are the density, the Young's modulus and the Poisson coefficient. Table 1 shows the linear material property values.

According to (Haar et al., 1984), the density of the water at temperature of 300°C is 727 kg/m³. If it is taken into account in the density of the steel C, the new “combined” or “equivalent” density increases from 7830 kg/m³ to 9121 kg/m³.

Figure 4 shows the nonlinear stress – plastic strain curves for different steel materials (A, B and C) used in the analyses. Material C is the most realistic one in this case. It is the normal austenitic stainless steel SS-2333 in operational temperature.

Table 1. Elastic material properties.

| Material | Steel (A, B) | Steel (C) | Concrete |
|--------------------------------------|--------------|-----------|----------|
| density, ρ [kg/m ³] | 7850 | 7830 | 2400 |
| Young's Modulus, E [GPa] | 210 | 176 | 35 |
| Poisson Coefficient, ν | 0.3 | 0.3 | 0.2 |

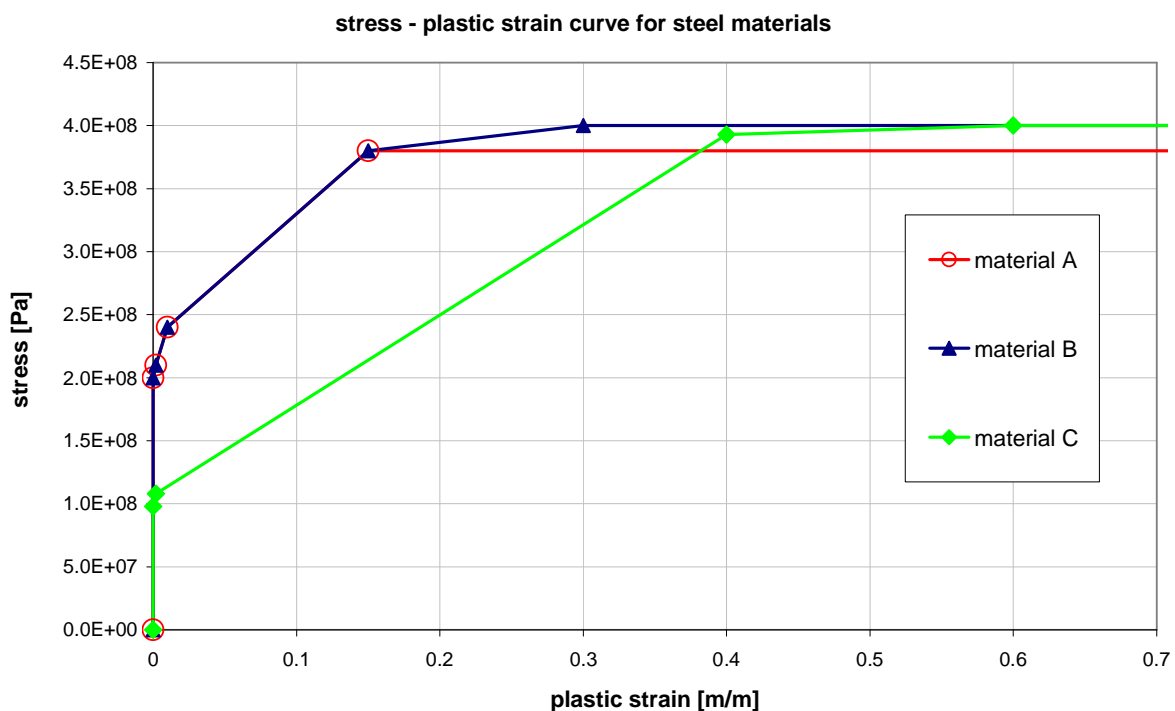


Figure 4. Stress – plastic strain curves for different steel materials (A, B and C) used in the analyses.

3.4 Boundary conditions

Both ends of the pipe are initially fixed. When the guillotine pipe break takes place at the upper left end, that end is released. In some analyses, the lower right end is given an acceleration transient (earthquake signal) in the in-plane horizontal direction of the wall to which the pipe is fixed (global 3-direction). All other degrees of freedom of both pipe ends are fixed.

In the elbow element model, three different types of special purpose elements are chosen to represent the restraint. Type A is a nonlinear spring element (SPRINGA) with a stiffness of 1 GN/m and a gap of 6 cm. The stiffness value was previously determined with a simulation of static compression of the part of structure in question. The nonlinearity comes from the fact that the spring acts only in tension (when the pipe is moving downwards) and only after the gap has been closed. There is no plasticity, i.e. no irrecoverable deformation or displacement of the spring end points. The spring is defined as follows:

```
*SPRING, NONLINEAR, elset=<element set name>
<blank line>
0., -0.5
0., 0.
0., 0.06
100.e6, 0.16
```

Type B is a nonlinear spring element (SPRINGA) with a gap of 6 cm. The spring acts only in tension (when the pipe is moving downwards) after the gap has been closed. The softening of the steel is taken into account by using the stress-strain curve of the steel material B. The spring is defined as follows:

```
*SPRING, NONLINEAR, elset=<element set name>
<blank line>
0., -0.5
0., 0.
0., 0.06
2.00E+06, 0.062
2.10E+06, 0.0627
2.40E+06, 0.0654
3.80E+06, 0.1088
4.00E+06, 0.154
4.20E+06, 0.3
```

The force remains constant outside the given range resulting in zero stiffness. That is why it is important to choose a range that is wide enough. Figure 5 shows the spring stiffness in the restraint element of type A and B as a force-displacement graph.

Type C restraint element is a pipe support element (ITSUNI). It represents a frame type of structure around the pipe where two parallel beams are in the opposite sides of the pipe. A linear spring element with a stiffness of 1 GN/m (which corresponds to type A nonlinear spring without any gap and with equal behaviour in both directions) is included to the pipe support element as a contact behaviour. In this study, the center of the pipe support element is chosen to coincide with the center of the pipe cross-section. The support beams are at 6 cm distance from the both sides of the pipe (upper and lower). Thus, the spring behaviour embedded in the pipe support element should be activated when the pipe has moved 6 cm in either direction. However, this was not the case and the gap was needed also within the spring behaviour.

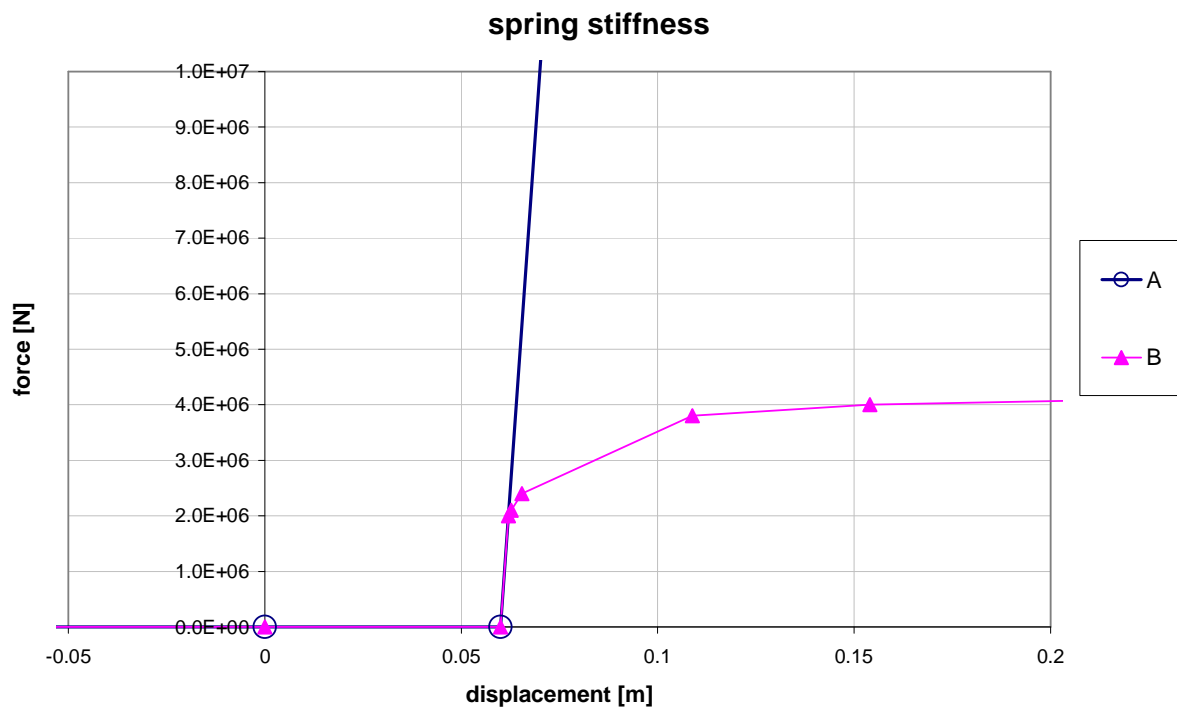


Figure 5. Spring stiffness in the restraint element of type A and B shown as a force-displacement graph.

3.5 Inner pressure

Two different pressures as functions of time are used. They are shown in Figure 6. The constant pressure was used in the studies reported previously. This time also a pressure which decreases from 15 MPa (or 150 bar) to 5 MPa (or 50 bar) in 1 ms is used. This kind of decrease very near the break point is based on several studies such as those by Haar et al. (1984), Robbe et al. (1999) and Brandt et al. (2008).

The constant pressure is used in the earthquake analysis described in Chapter 6.

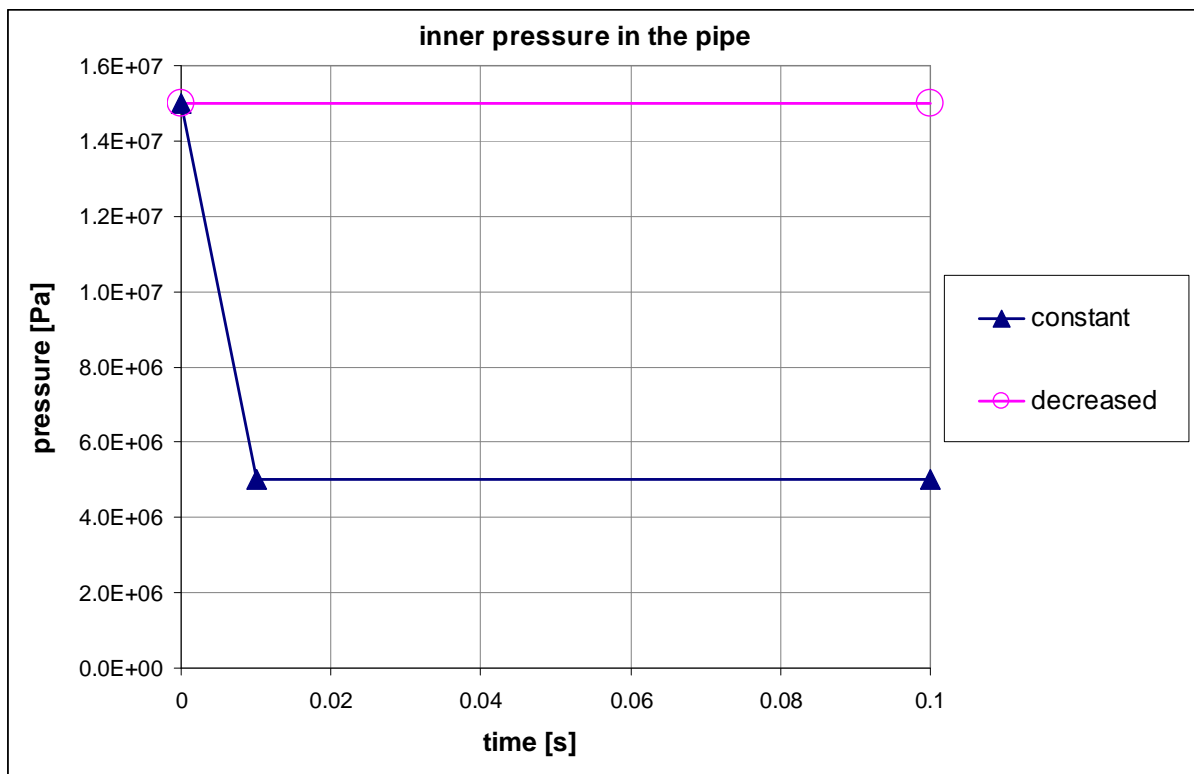


Figure 6. Inner pressure in the pipe as a function of time after the pipe break.

4 Dynamic analysis of a guillotine pipe break with old parameters

A guillotine pipe break is chosen as a nonlinear dynamic analysis case. It is first analysed using the combined model shown lowermost in Figure 2. That is a relatively large model with shell elements for the pipe which was chosen based on the eigenfrequency results in the previous study (Calonius, 2008) and solid volume elements for the concrete and the steel restraint. After that, as a comparison, the same case is analyzed with a model using only structural and special-purpose elements; elbow elements for the pipeline and a nonlinear spring element for the support. The properties such as the stiffness of the spring element are determined by preliminary static analyses with the large combined model. Nonlinear spring element (SPRINGA) with a stiffness of 1 GN/m and a gap of 6 cm is used.

The release of fluid from a break in high-energy piping can result in significant changes in flow characteristic within the piping system, creating reaction forces, which dynamically excite the piping. If these forces are sufficient to cause a pipe whip, nearby required systems must be protected or designed to withstand the result of the pipe whip. In reactor primary circuit, it is also important to keep the break flow area and thus the outflow of the coolant limited in case of pipe break.

The fluid forces acting on the ruptured pipe are a function of time and space, and depend on the fluid state within the pipe prior to rupture, the break flow area, frictional losses, and plant system characteristics. Break flow area is often assumed to develop within one millisecond after break initiation. Fluid forces can be divided into two parts: initial thrust force and steady state thrust force. The former is:

$$F_{in} = P_0 A_e \quad (\text{Equation 1})$$

where P_0 is the initial pressure in the pipe and A_e the break plane area. The steady state thrust coefficient is dependent on the fluid state and the frictional effects. In this present case with the new geometry, the initial thrust force is 9.54 MN.

Normally, a dynamic time history analysis shall be conducted of the ruptured piping to determine its response to the exciting forces. The pipe whip constraints and other objects that can modify the pipe whip motion shall be considered in the analysis. Absorption of energy via plastic pipe deformation is typically the most desirable method in the design of piping and restraints for protection against pipe whip effects. The elastic and plastic behaviour of the pipe material shall be taken into account in the analysis (Vörös, 2002) (Micheli, 2003).

According to a study by Robbe et al. (1999) there are three phases of pressure drop in a PWR Primary Circuit pipe break. During the first 5 ms, pressure drops from 155 bar to around 70 bar. When it gets to the saturation pressure, the water vaporizes. The flow rate increases until it has reached the critical flow rate. From 5 ms to 100 ms, a general pressure loss to around 80 bar takes place in the whole circuit. After 100 ms, a slow diphasic pressure decrease takes place in the whole circuit. In this study, fluid-structure interaction (FSI) phenomena were not taken into account.

In an article by (Brandt et al., 2008), a large-break loss of coolant accident (LBLOCA) where a guillotine break of one of the main coolant pipes occurs near the reactor pressure vessel (RPV) was studied. LBLOCA initiates a pressure wave which propagates inside the RPV. The simulation of bidirectional FSI phenomena was found to be important for accurate prediction of the resulting deformation and loads. Fully coupled simulation results were validated against the German HDR (Heißdampfreaktor) experiments. Regarding the pressure near the break point, however, results by Robbe et al. and Brandt et al. are in agreement with each other. Of course, the first milliseconds are sensitive to the assumed pipe break opening time and rate.

The analyses in this study consist of two steps. The first step is static during which an inner pressure is applied to the pipe. It is linearly ramped up within one second. The upper end and the lower right end of the pipe are fixed during this step. The second step is dynamic with automatic time incrementation. Right in the beginning of it the free end is released, which initiates the pipe break condition instantaneously.

Table 2 presents a list of all the six nonlinear dynamic analysis cases studied in the previous report (Calonius, 2009a). They are also reported in the paper (Calonius, 2009b). Element, material and analysis (time integration) types are varied. In these analyses, the same inner pressure remains throughout the second step even though in reality the pressure decreases at some rate when the water bursts out from the free end. Thus, the analyses are conservative in many ways. In this present study, the analyses were done in a more detailed manner. The new cases, although with the same old geometry, are listed in Table 3. In fact, case O1 is exactly the same as the old case EPI, only solved now with a more recent version of Abaqus. After that, some parameters or characteristics of the analysis are systematically varied in cases from O1 to O5.

The strain rate sensitivity of the steel is taken into consideration by the Cowper-Symonds equation:

$$\sigma_{yd} = \sigma_y \left[1 + \left(\frac{\dot{\epsilon}}{D} \right)^{1/q} \right],$$

where σ_y and σ_{yd} are the static and the dynamic yield stress, respectively, and D and q are material parameters. Strain rate dependency parameter values $D = 1522$ and $q = 5.13$ are used.

Table 2. Dynamic analysis cases studied in the previous report (Calonius, 2009a).

| Case code | Main element type | Main material type | Analysis type | Analysis time (dynamic step) | CPU time |
|-----------|-------------------|--------------------|---------------|------------------------------|----------|
| SEI | Shell | Elastic | implicit | 1.00 s | 48 418 s |
| SEE | Shell | Elastic | explicit | 1.00 s | 25 491 s |
| SPI | Shell | Plastic | implicit | 0.30 s | 75 148 s |
| SPE | Shell | Plastic | explicit | 0.26 s | 22 887 s |
| EEl | Elbow | Elastic | implicit | 2.00 s | 565 s |
| EPI | Elbow | Plastic | implicit | 0.22 s | 274 s |

Table 3. Analysis cases with the old pipe dimensions and pressure.

| Case | Element type | Material | Rate dependence | Pressure | Spring | Mass of water |
|------|--------------|----------|-----------------|----------|--------|---------------|
| O1 | Elbow | A | No | Constant | A | No |
| O2 | Elbow | B | No | Constant | A | No |
| O3 | Elbow | C | No | Constant | A | No |
| O4 | Elbow | C | Yes | Constant | A | No |
| O5 | Elbow | C | Yes | Drop | A | No |

Figure 7 shows the energy balance during the analysis of case O1. It is maintained until the pipe has deformed too radically after it has impacted to the restraint. Figure 8 shows the vertical forces as functions of time in the right pipe end (green), in the left end (blue) and in the fixed end of the spring (orange). The pipe hits the restraint 0.02 s after the initiation of the pipe break. The analysis terminates 0.2 s after that. The maximum force in the spring is 18 MN.

Figure 9 shows the energy balance during the analysis of case O2. It is maintained until the pipe has deformed too radically after it has impacted to the restraint. Figure 10 shows the vertical forces as functions of time in the right pipe end (green), in the left end (blue) and in the fixed end of the spring (orange). The pipe hits the restraint 0.02 s after the initiation of the pipe break. The analysis terminates 0.11 s after that. The maximum force in the spring is almost 19 MN.

Figure 11 shows the energy balance during the analysis of case O3. It is maintained until the pipe has deformed too radically after it has impacted to the restraint. Figure 12 shows the vertical forces as functions of time in the right pipe end (green), in the left end (blue) and in the fixed end of the spring (orange). The pipe hits the restraint 0.02 s after the initiation of the pipe break. The analysis terminates 0.09 s after that. The maximum force in the spring is 14 MN.

Figure 13 shows the energy balance during the analysis of case O4. It is maintained until the pipe has deformed too radically after it has impacted to the restraint. Figure 14 shows the vertical forces as functions of time in the right pipe end (green), in the left end (blue) and in the fixed end of the spring (orange). The pipe hits the restraint 0.02 s after the initiation of the pipe break. The analysis terminates 0.14 s after that. The maximum force in the spring is 16 MN.

Figure 15 shows the energy balance during the analysis of case O5. It is maintained. Figure 16 shows the vertical forces as functions of time in the right pipe end (green), in the left end (blue) and in the fixed end of the spring (orange). The pipe hits the restraint 0.03 s after the initiation of the pipe break. The analysis is completed and not terminated. The maximum force in the spring is 7.5 MN. This analysis included the decreasing inner pressure, which has a notable effect on the behaviour of the pipe. There is no formation of the plastic hinge.

Figure 17 shows the force in the spring as a function of time in all covered cases.

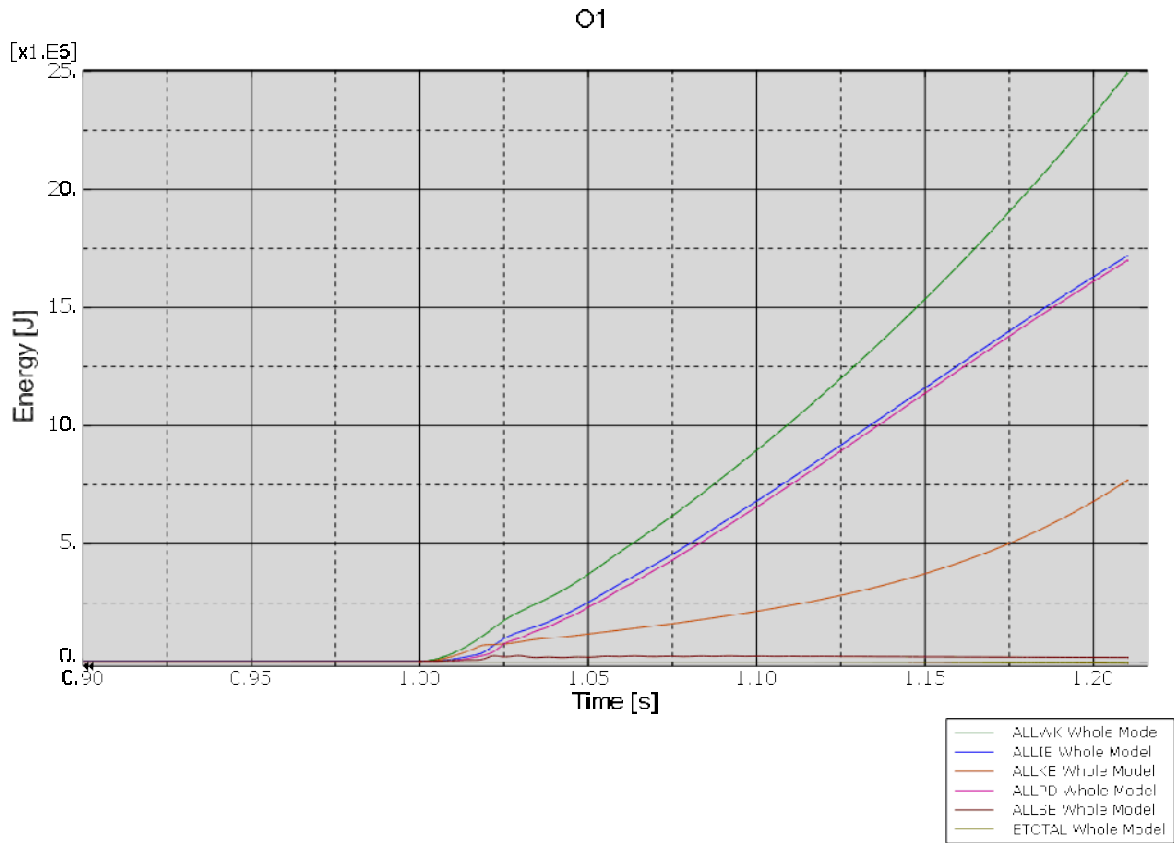


Figure 7. Energy balance (O1).

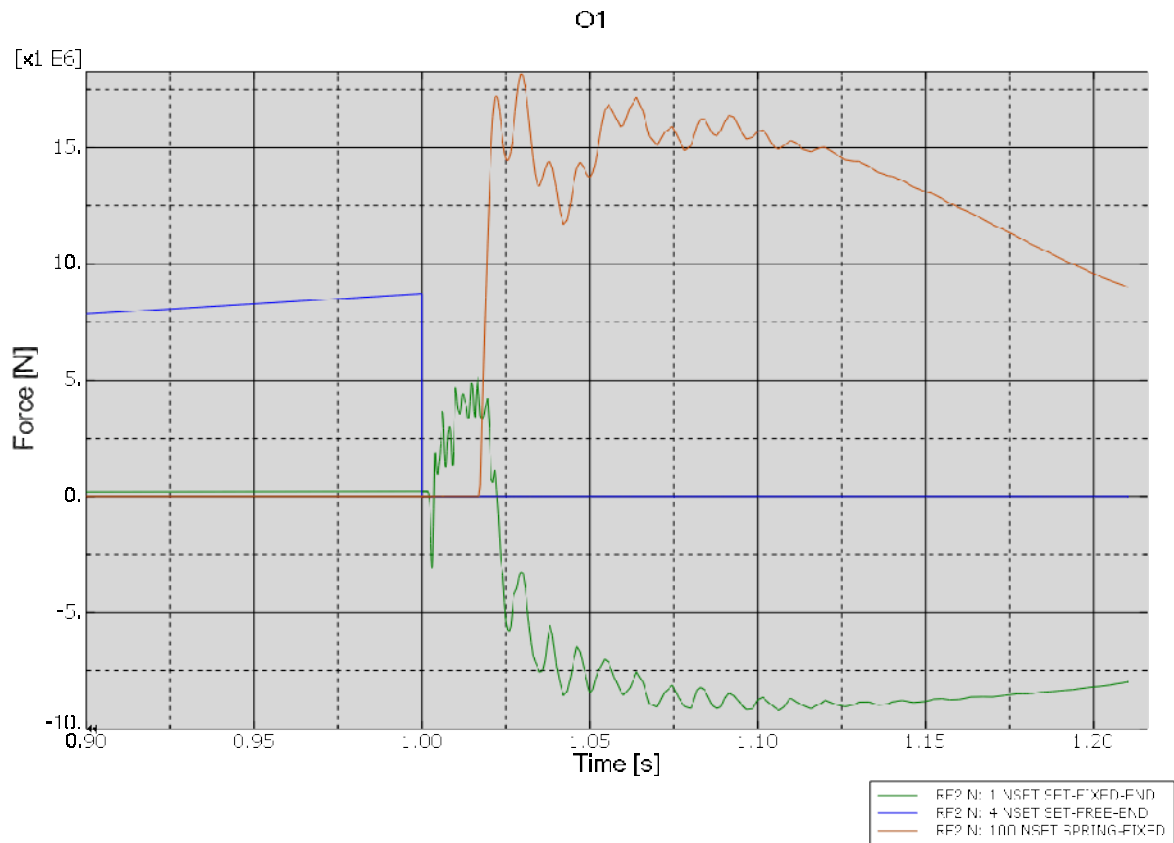


Figure 8. Vertical forces as functions of time in the right pipe end (green), in the left end (blue) and in the fixed end of the spring (orange) (O1).

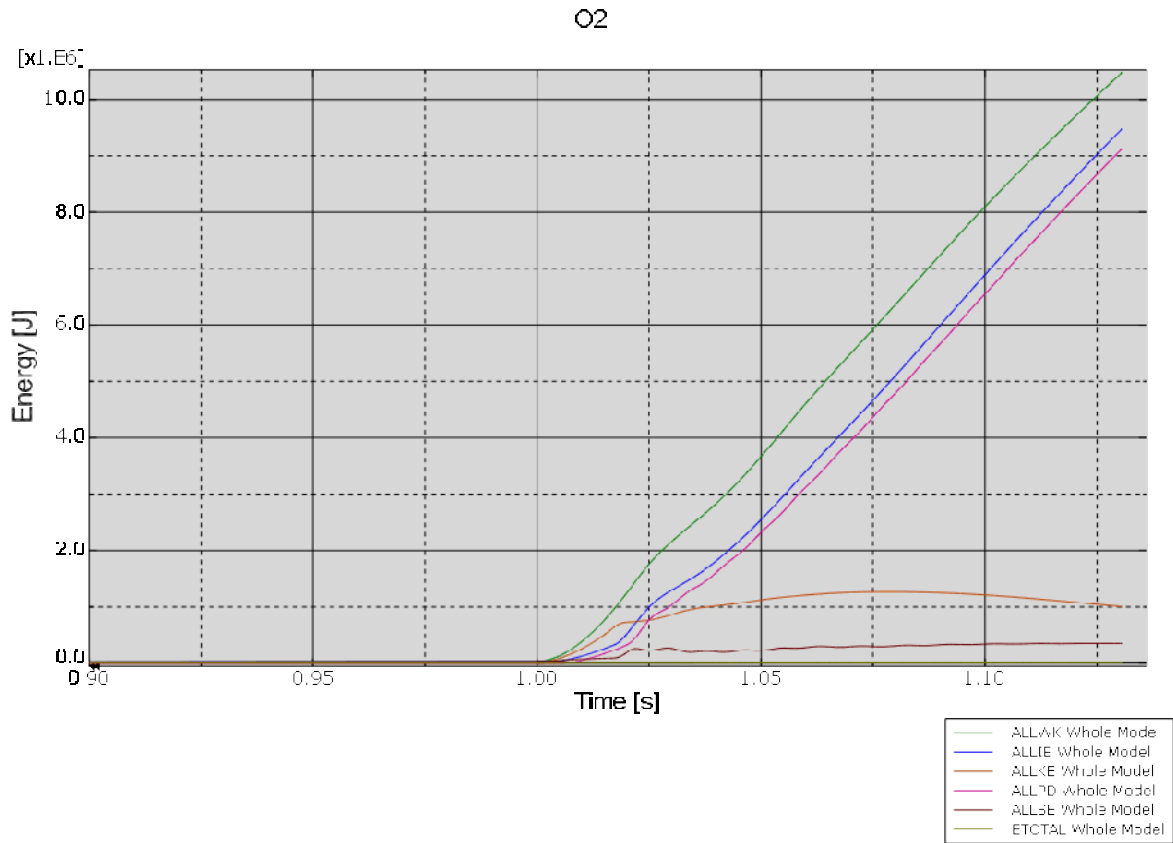


Figure 9. Energy balance (O2).

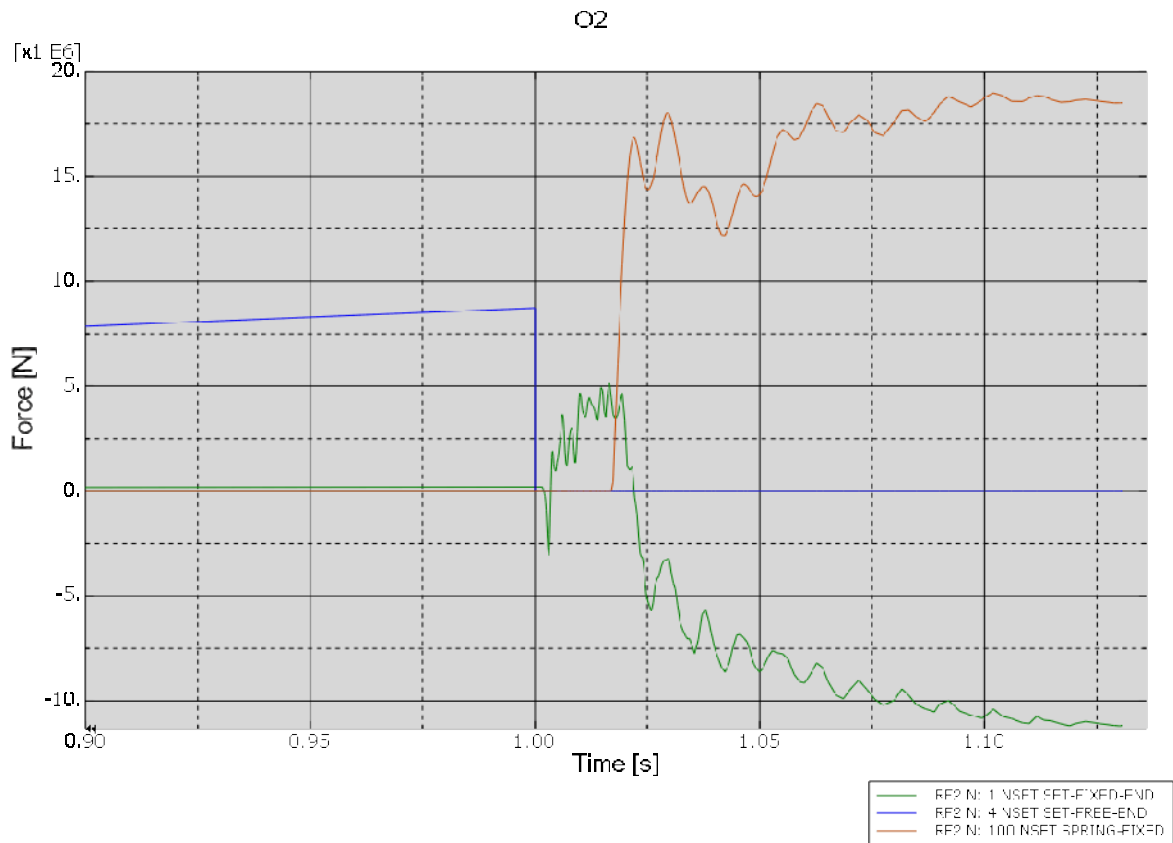


Figure 10. Vertical forces as functions of time in the right pipe end (green), in the left end (blue) and in the fixed end of the spring (orange) (O2).

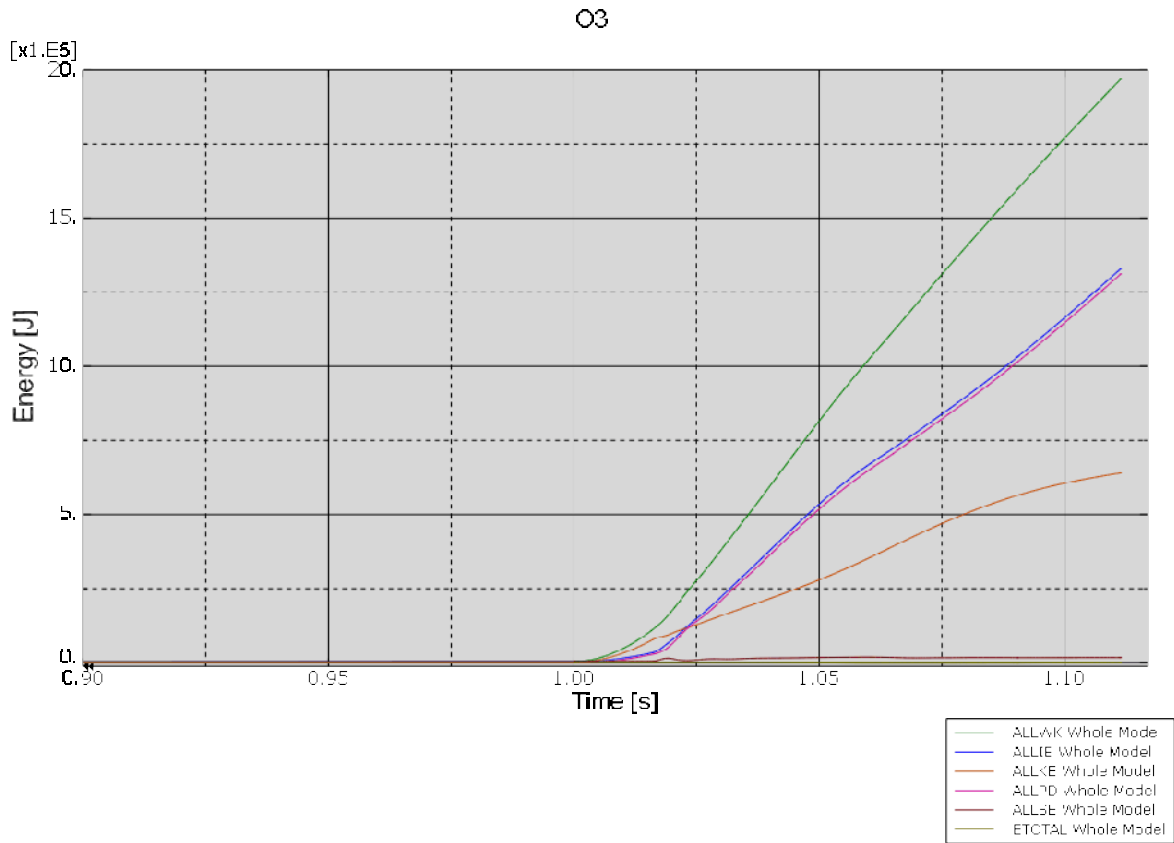


Figure 11. Energy balance (O3).

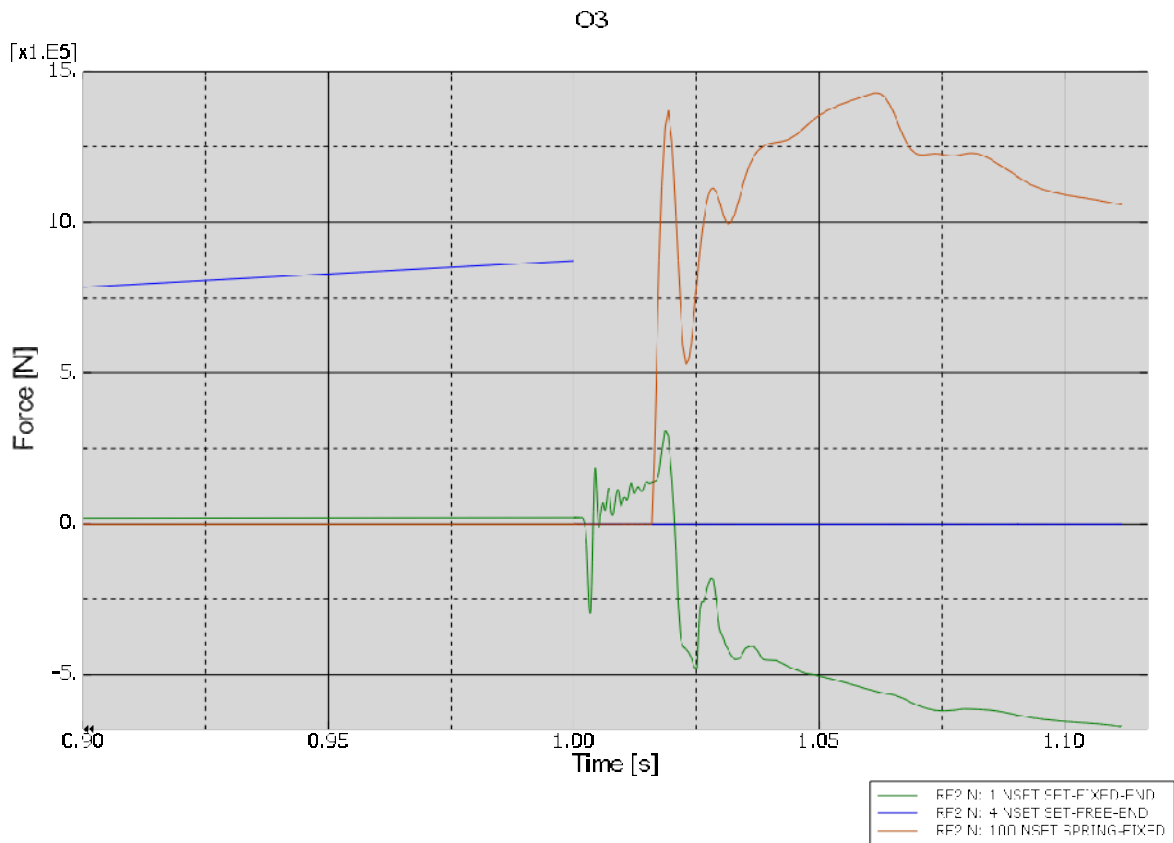


Figure 12. Vertical forces as functions of time in the right pipe end (green), in the left end (blue) and in the fixed end of the spring (orange) (O3).

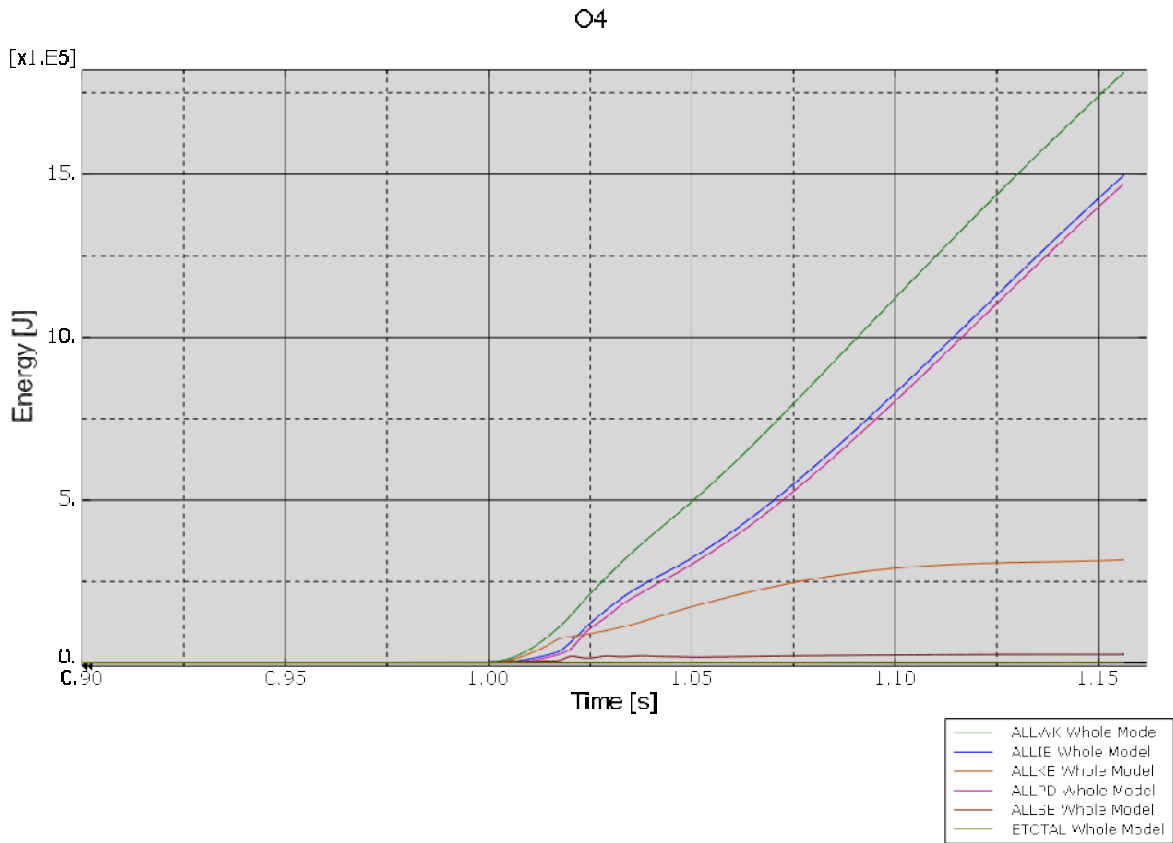


Figure 13. Energy balance (O4).

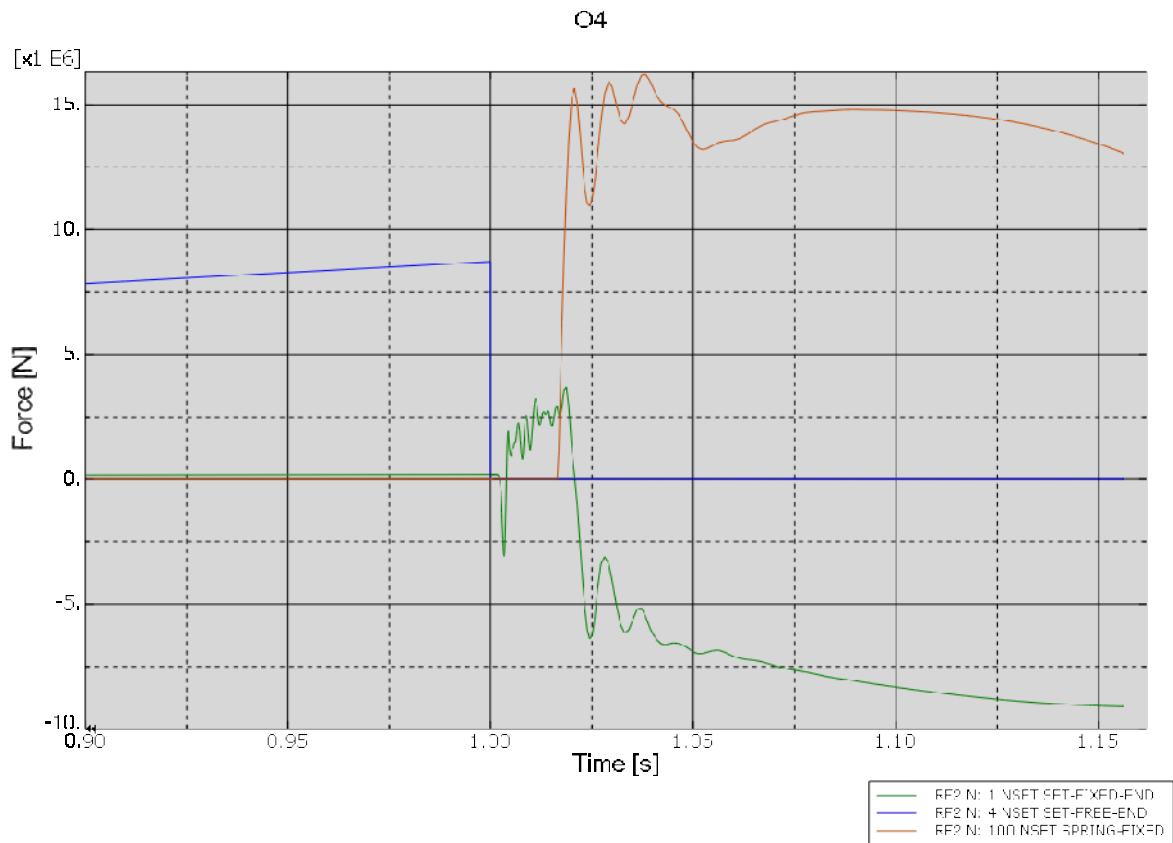


Figure 14. Vertical forces as functions of time in the right pipe end (green), in the left end (blue) and in the fixed end of the spring (orange) (O4).

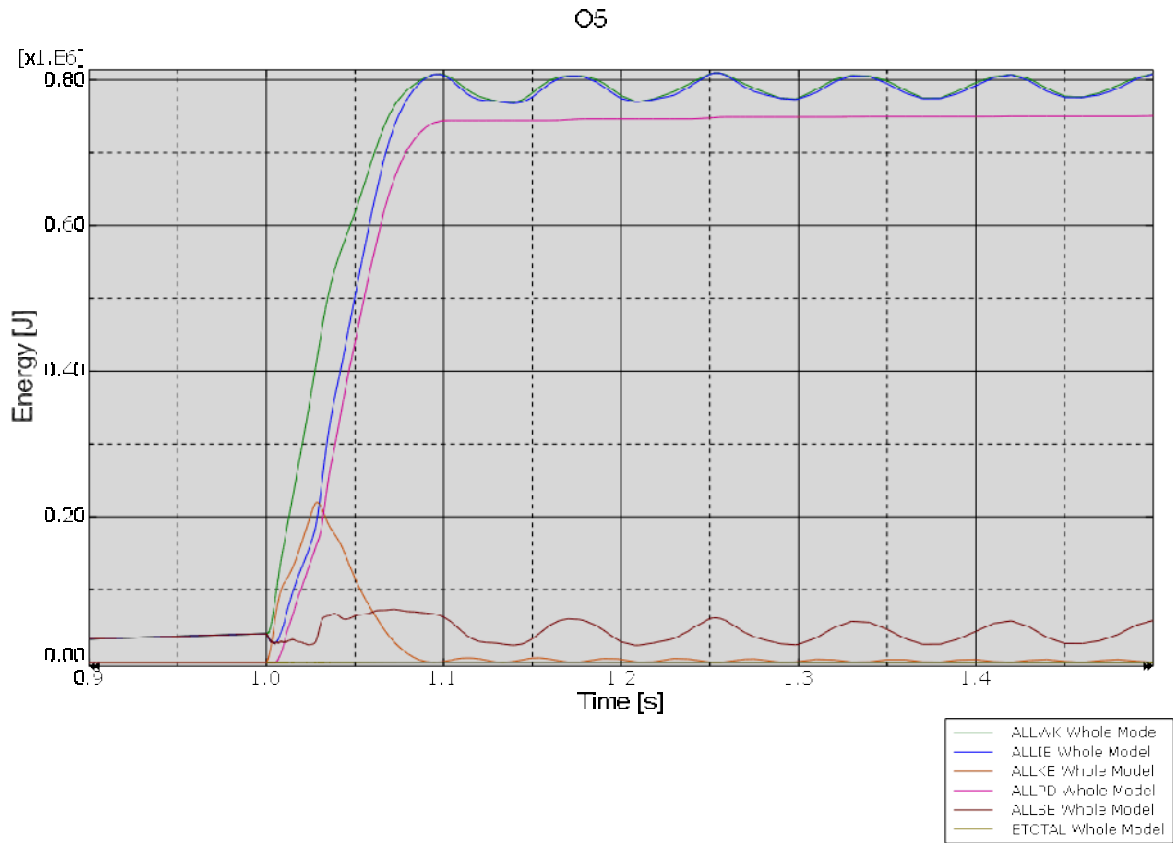


Figure 15. Energy balance (O5).

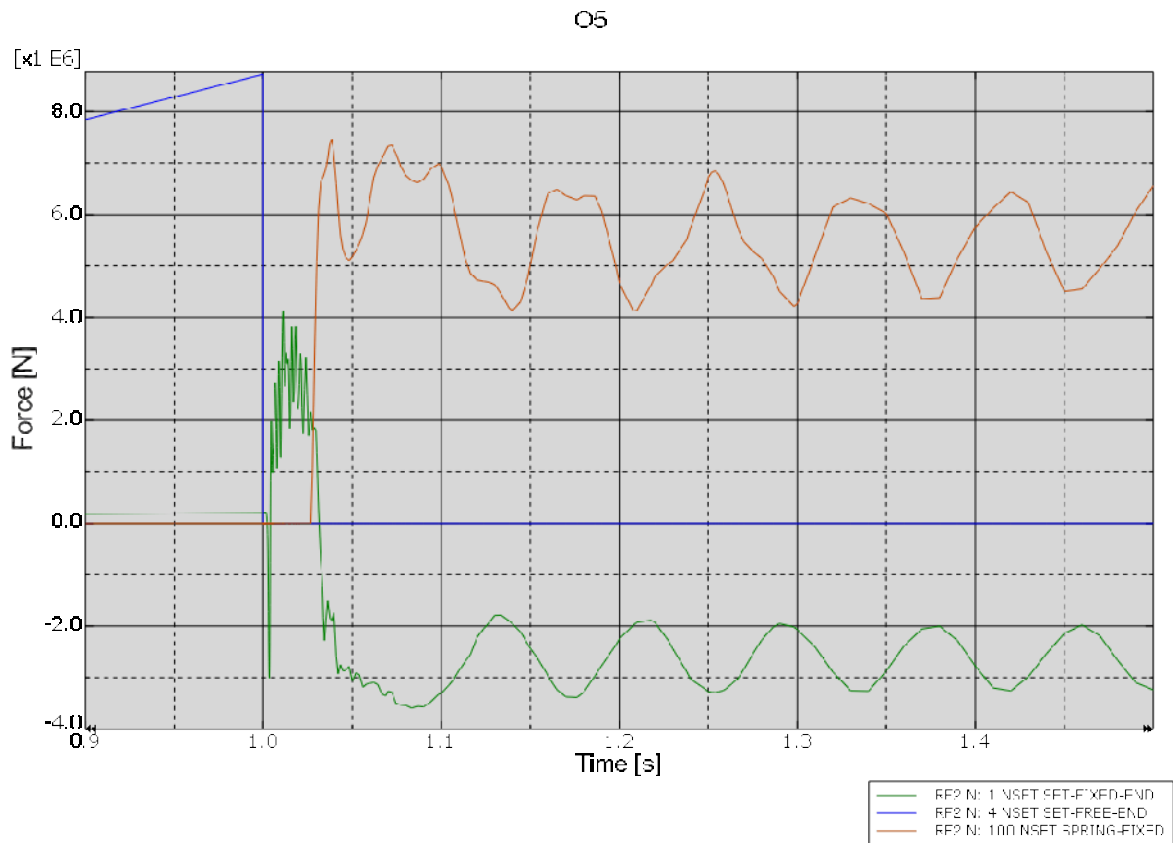


Figure 16. Vertical forces as functions of time in the right pipe end (green), in the left end (blue) and in the fixed end of the spring (orange) (O5).

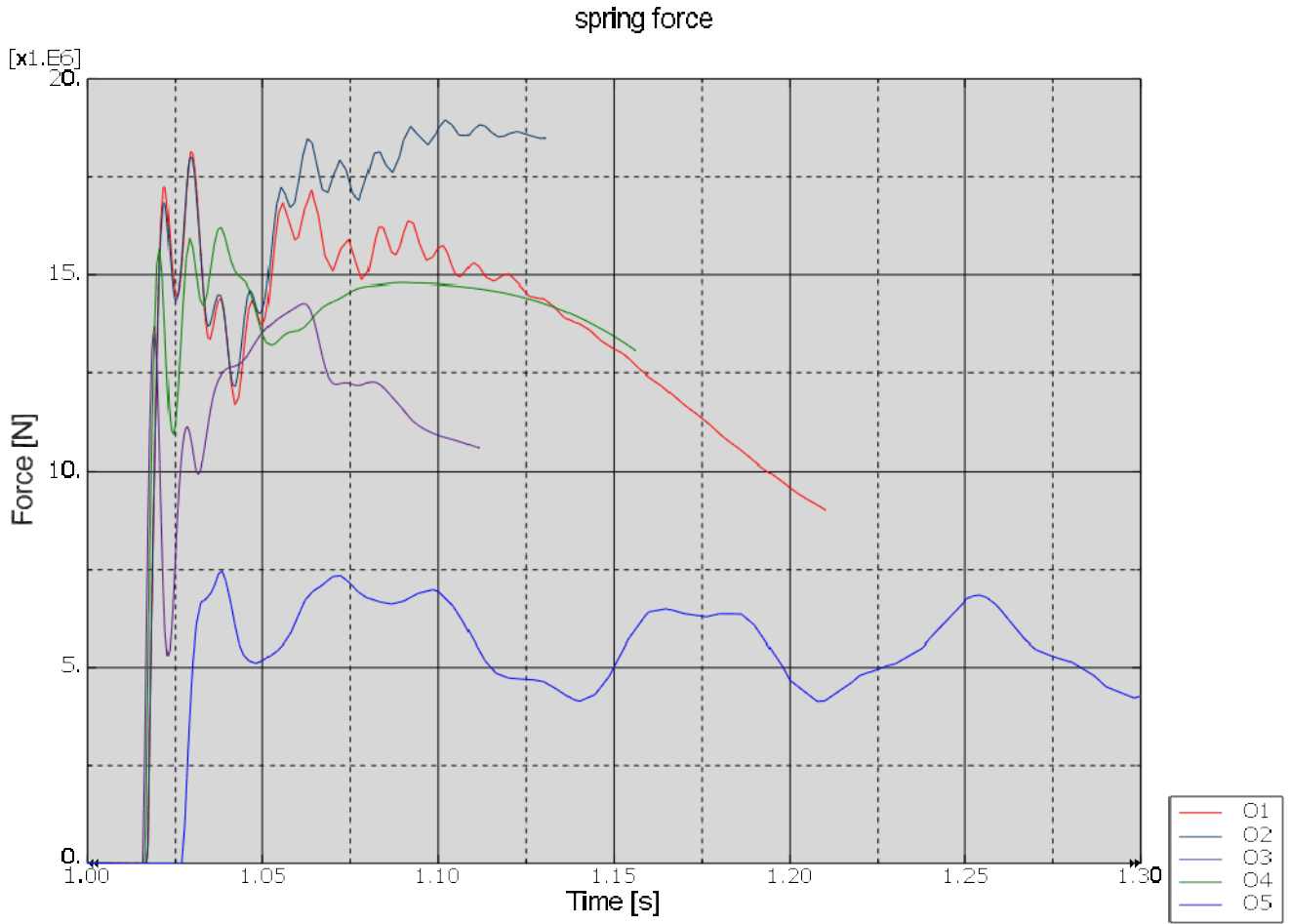


Figure 17. The force in the spring as a function of time in all covered cases.

5 Dynamic analysis of a guillotine pipe break with new parameters

The pipe dimensions and the inner pressure are slightly changed for the new analyses. They are also conducted with Abaqus/Standard version 6.9-2. Table 4 shows the new pipe break cases. Also an analysis with the shell element model is conducted with the new parameters (case N2). Case N1 is otherwise the same as O5, but with new dimensions. The spring of type C in the table (in case N4) means ITSUNI element with an incorporated spring of type A.

Table 4. Pipe break cases with the new dimensions and pressure.

| Case | Element type | Material | Rate dependence | Pressure | Spring | Mass of water |
|------|--------------|----------|-----------------|----------|--------|---------------|
| N1 | Elbow | C | Yes | drop | A | No |
| N2 | Shell | C | Yes | drop | - | No |
| N3 | Elbow | C | Yes | drop | B | No |
| N4 | Elbow | C | Yes | drop | C | No |
| N5 | Elbow | C | Yes | drop | A | Yes |

Figure 18 shows the energy balance during the whole analysis in case N1. It is maintained. Figure 19 shows the same results for the first 0.3 s of the pipe break. Figure 20 shows the vertical forces as functions of time in the right pipe end (blue), in the left end (green) and in the fixed end of the spring (red). Figure 21 shows the same results for the first 0.3 s of the pipe break. The pipe hits the restraint about 0.04 s after the initiation of the pipe break. The analysis is completed and not terminated. The maximum force in the spring is 11 MN. This analysis included the decreasing inner pressure, which has a notable effect on the behaviour of the pipe. That was already shown in the previous chapter with the old parameters. There is no formation of the plastic hinge.

Figure 22 shows the energy balance during the first 0.3 s of the pipe break in case N2, as obtained with the shell element model. It is maintained. Figure 23 shows the vertical displacements in various locations at the restraint as functions of time. When the pipe has moved 6 cm downwards, it hits the restraint. The steel part of the restraint deforms about 2 cm. The concrete (with linear elastic properties) deforms about 0.3 cm. Figure 24 shows the vertical forces as functions of time in the right pipe end (blue) and in the bottom of the restraint (red) during the first 0.3 s of the pipe break. The pipe hits the restraint about 0.04 s after the initiation of the pipe break. The analysis is completed and not terminated. The maximum force measured from the bottom of the concrete block is slightly over 5 MN, which is considerably less than in the case with the spring element (case N1). The forces in the pipe end are of the same order.

Figure 25 shows the energy balance during the first 0.3 s of the pipe break in case N3. It is maintained. Figure 26 shows the vertical forces as functions of time in the right pipe end (blue) and in the fixed end of the spring (red) during the first 0.3 s of the pipe break. The pipe hits the restraint about 0.04 s after the initiation of the pipe break. The analysis is completed and not terminated. The maximum force in the spring is slightly less than 4 MN. This analysis included the decreasing inner pressure and also the effect of material softening incorporated in the spring behaviour. There is no formation of the plastic hinge. After reaching the maximum level, the spring force stays constant, which is rather unrealistic.

Figure 27 shows the energy balance during the first 0.3 s of the pipe break in case N4. It is maintained. Figure 28 shows the vertical displacements as functions of time in the free end (darker line) and in the pipe at the restraint (lighter line) for the duration of the whole analysis. This analysis corresponds to the case N1, but the SPRINGA element is replaced with an ITSUNI element. Also, the results of those two cases are in a very close agreement. The pipe hits the restraint about 0.04 s after the initiation of the pipe break. The gap is approximately 6 cm also in case N4. The analysis is completed and not terminated. The maximum force in the spring is 11 MN. Some comparison is shown further in Figure 32.

Figure 29 shows the energy balance during the first 0.3 s of the pipe break in case N5. It is maintained. The mass of water is taken into account. Some comparison is shown later in Figure 33.

Next, different cases are compared with each other. Figure 30 shows the vertical displacements of different locations at the restraint as functions of time in cases N1, N2 and N3. Regarding the maximum displacements, the behaviour in case N2 is somewhere between those in cases N1 and N3. Regarding the vibration amplitude, case N2 is slightly closer to case N1. Case N2 has a quite extensive shell element model and can be considered the most accurate one of these cases. This figure clearly shows, that even though the spring of type B in case N3 has nonlinear softening kind of force-displacement response, the displacement is recoverable and does not correspond in that sense to the real plastic deformation of a steel restraint.

Figure 31 shows the vertical forces as functions of time in the restraint or spring in cases N1, N2 and N3. The force in case N3 stays in a value of approximately 3.85 MN. According to the force-displacement response of the type B spring, the corresponding displacement should be approximately 11 cm and Figure 30 shows, that in fact, the displacement oscillates around that value.

Figure 32 shows the vertical forces as functions of time in the right pipe end and in the fixed end of the type A spring in cases N1 and N4. It is shown that the SPRINGA and ITSUNI elements behave similarly when they are given corresponding parameter values. There is virtually no difference in the behaviour. Figure 33 shows the vertical forces as functions of time in the right pipe end and in the fixed end of the type A spring in cases N1 and N5. It is shown that the mass of the water plays only a minor role in the dynamic behaviour of the pipe in this kind of case. The response is slightly slower with more mass. There is 16% more mass in the system and the impact takes place after about the same relative duration. The maximum forces are almost the same. It seems that the inner pressure is the governing factor when it comes to the forces transferred by the supports.

Figure 34 shows the deformed shape and the equivalent plastic strain as a contour plot 1 second after the pipe break in case N2. Values over 1% are in dark red colour. Figure 35 shows a detail plot of that with a different contour scale. Values over 5% are in dark red colour. Figure 36 shows the equivalent plastic strain 1.0 seconds after the pipe break in case N4. The contour scale is the same as in Figure 34. The pipe support element (ITSUNI) is shown in black. Deformations are scaled up by a factor of 10. These figures are difficult to compare with each other quantitatively. In Figure 36, the strain contour is from the inner surface of the pipe extrados. In Figures 34 and 35, the strain contour is from the inner surface. In the elbow element model, there are no such local peaks as in the shell element model.

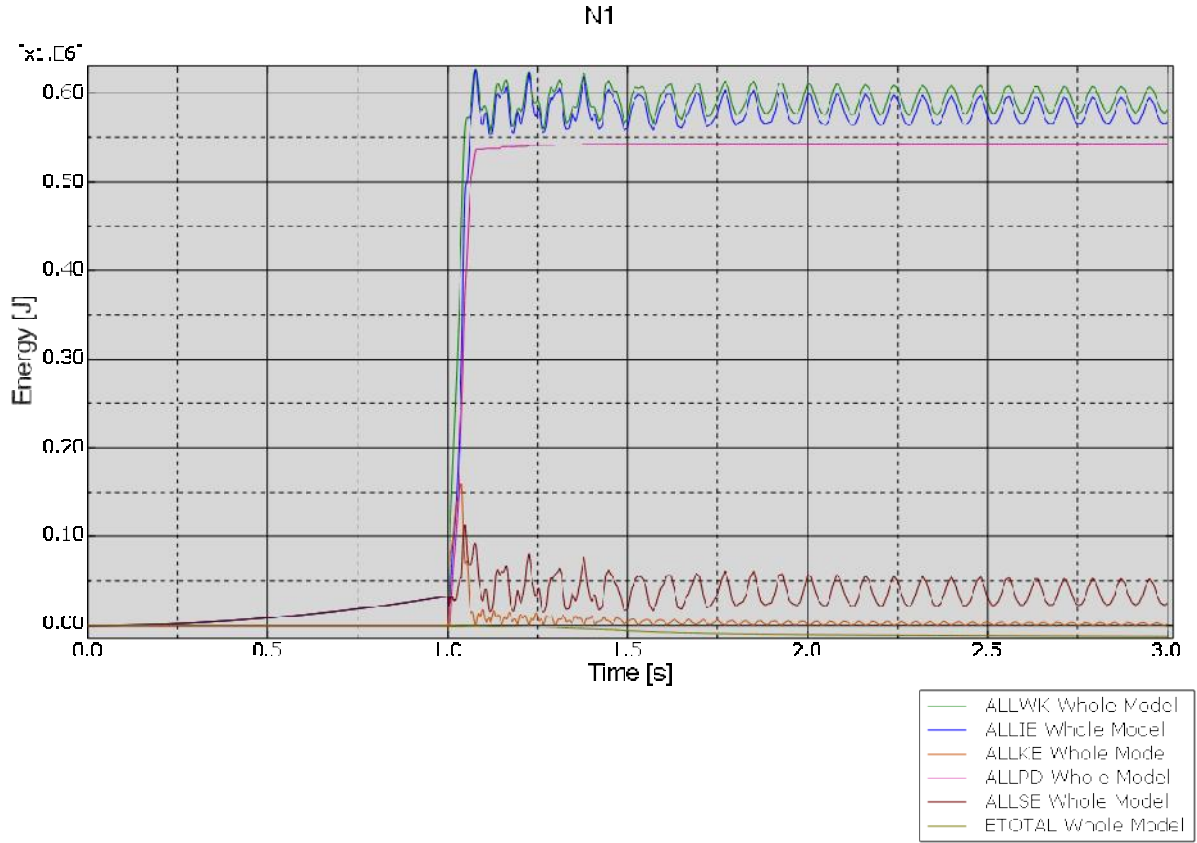


Figure 18. Energy balance during the whole analysis (N1).

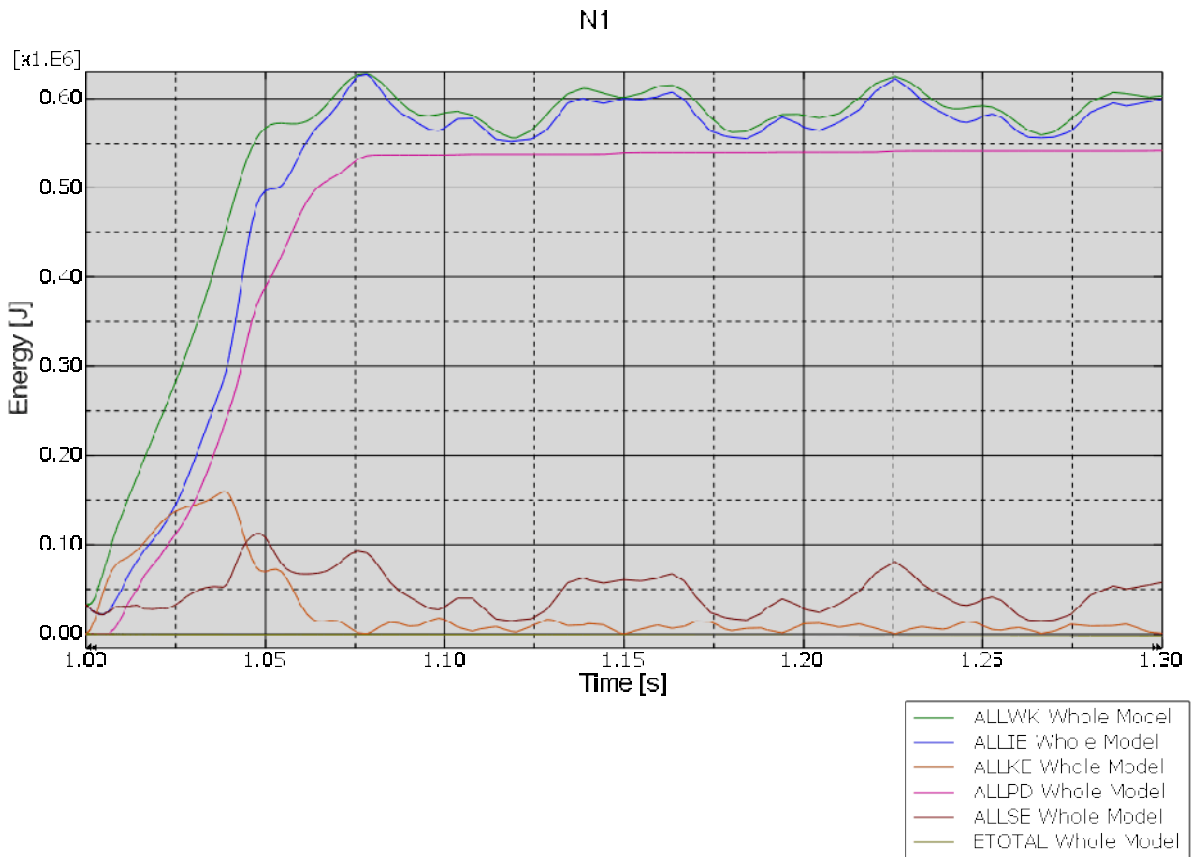


Figure 19. Energy balance during the first 0.3 s of the pipe break (N1).

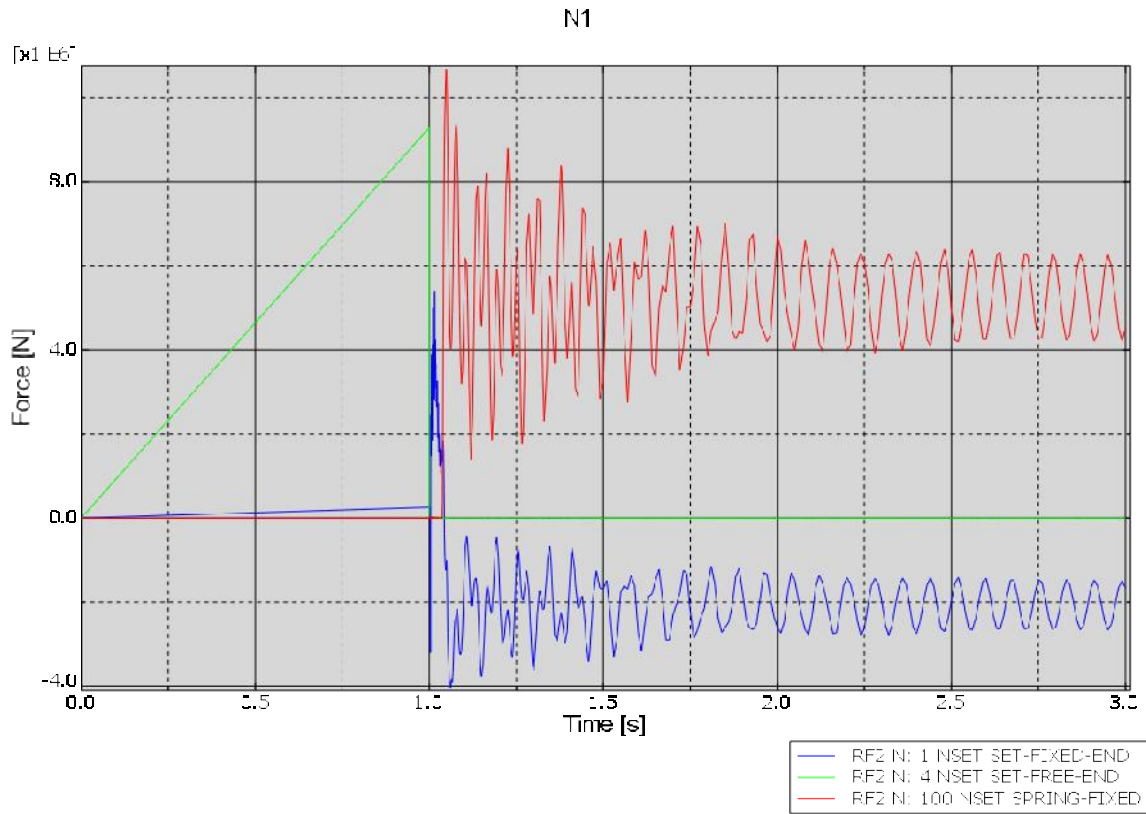


Figure 20. Vertical forces as functions of time during the whole analysis in the right pipe end (blue) and in the fixed end of the type A spring (red) (N1).

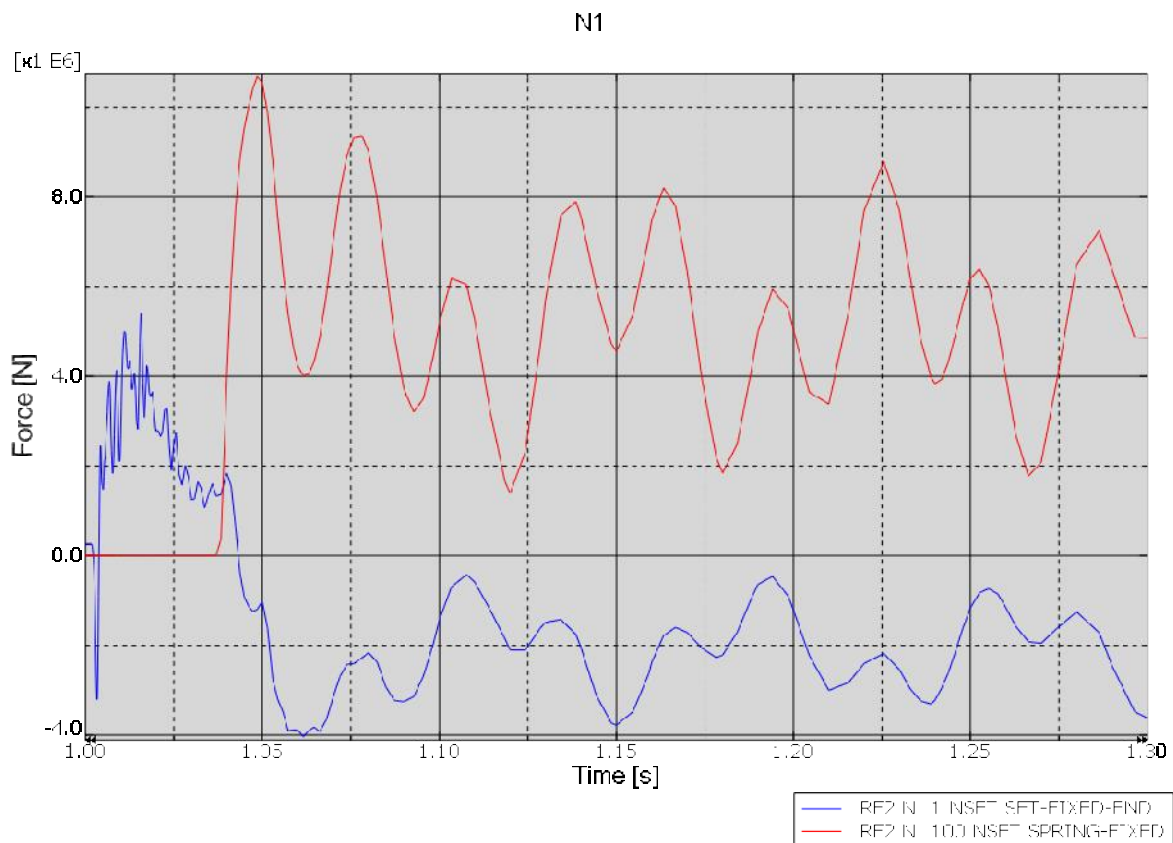


Figure 21. Vertical forces as functions of time during the first 0.3 s of the pipe break in the right pipe end (blue) and in the fixed end of the type A spring (red) (N1).

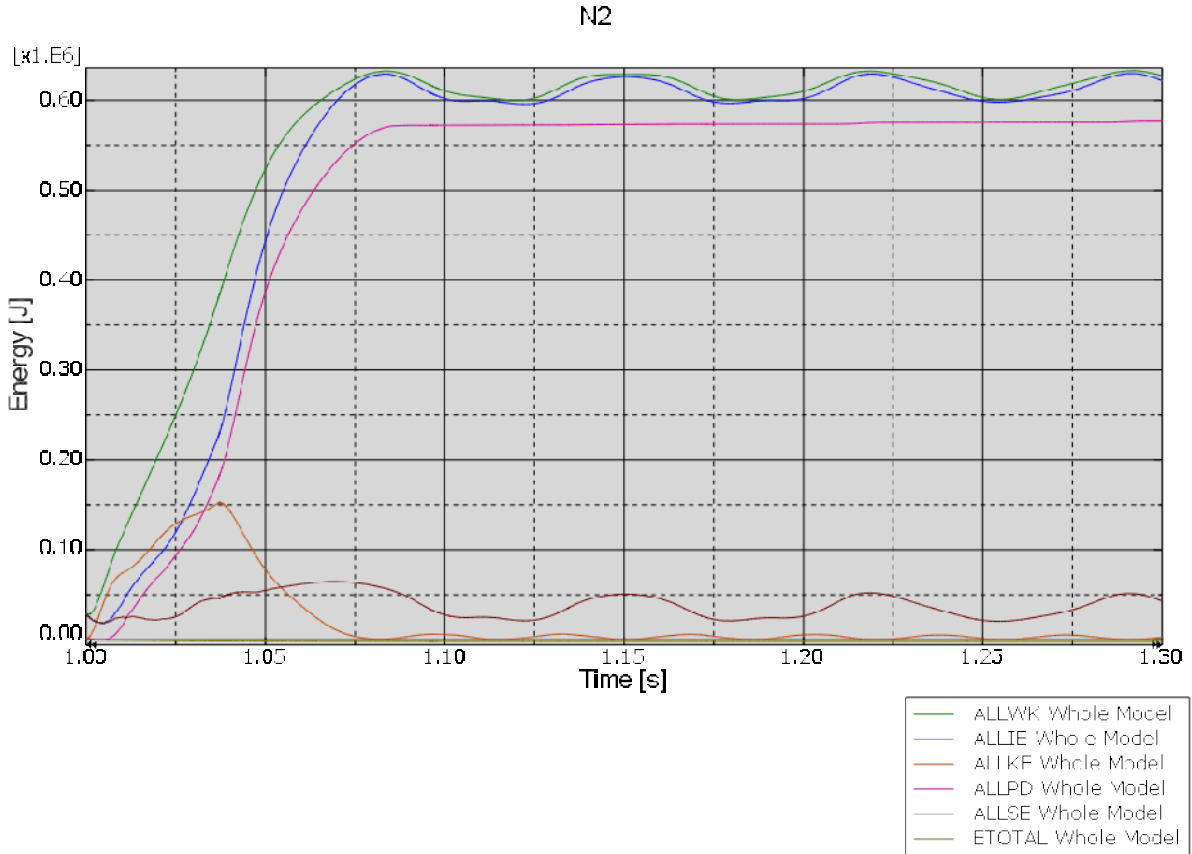


Figure 22. Energy balance (N2).

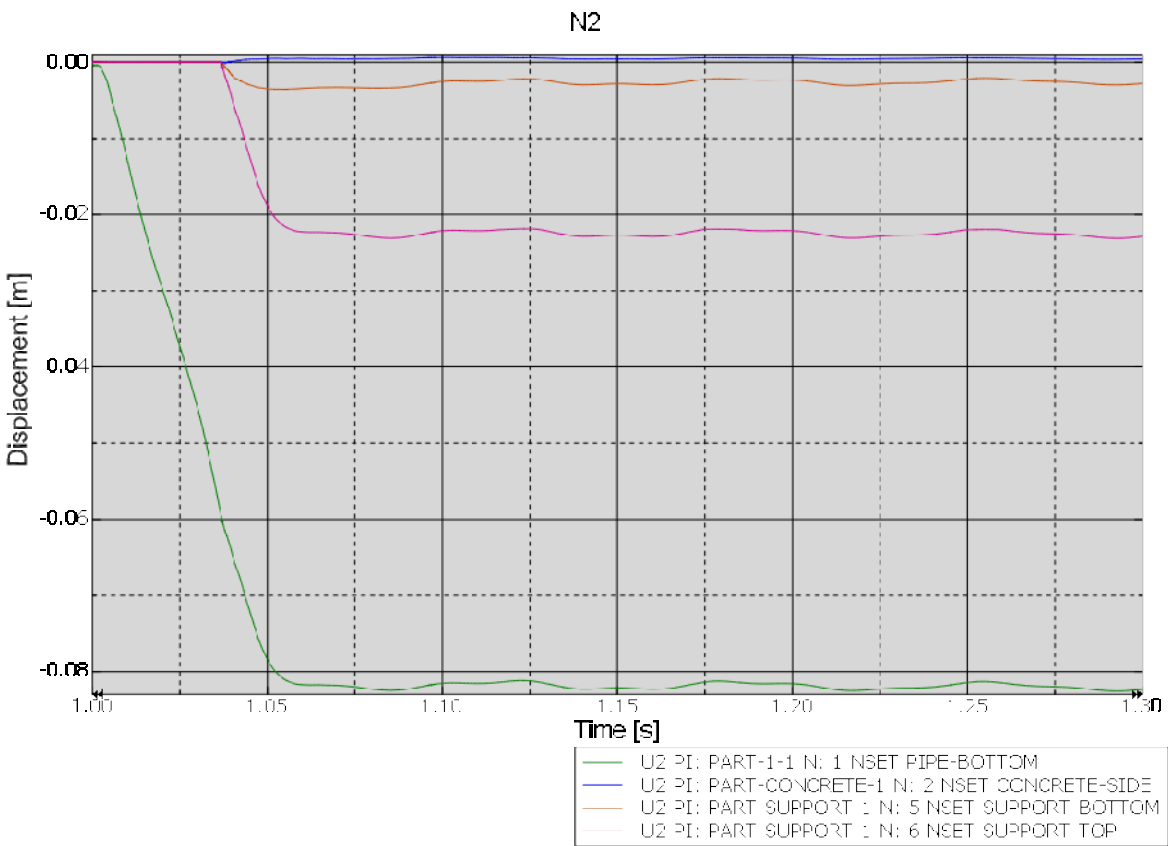


Figure 23. Vertical displacements of different locations at the restraint as functions of time (N2).

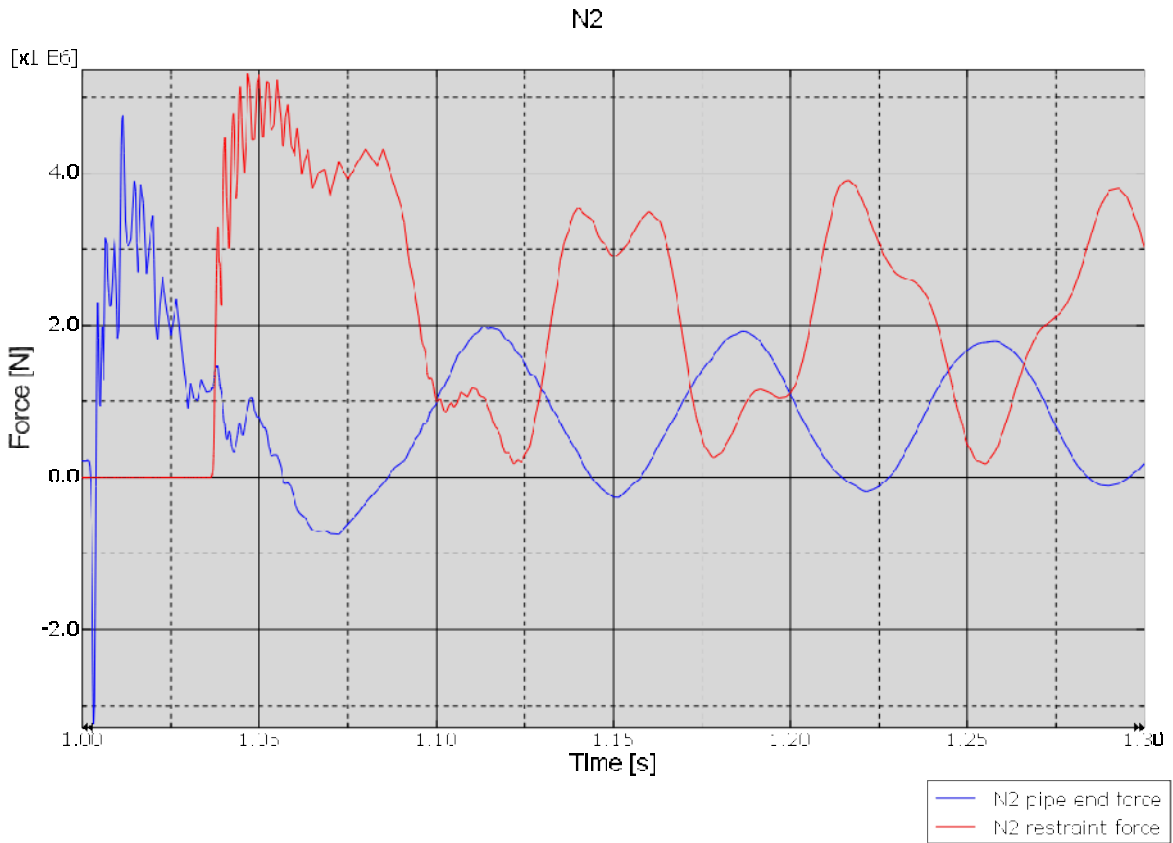


Figure 24. Vertical forces as functions of time in the right pipe end (blue) and in the bottom of the restraint concrete block (red) (N2).

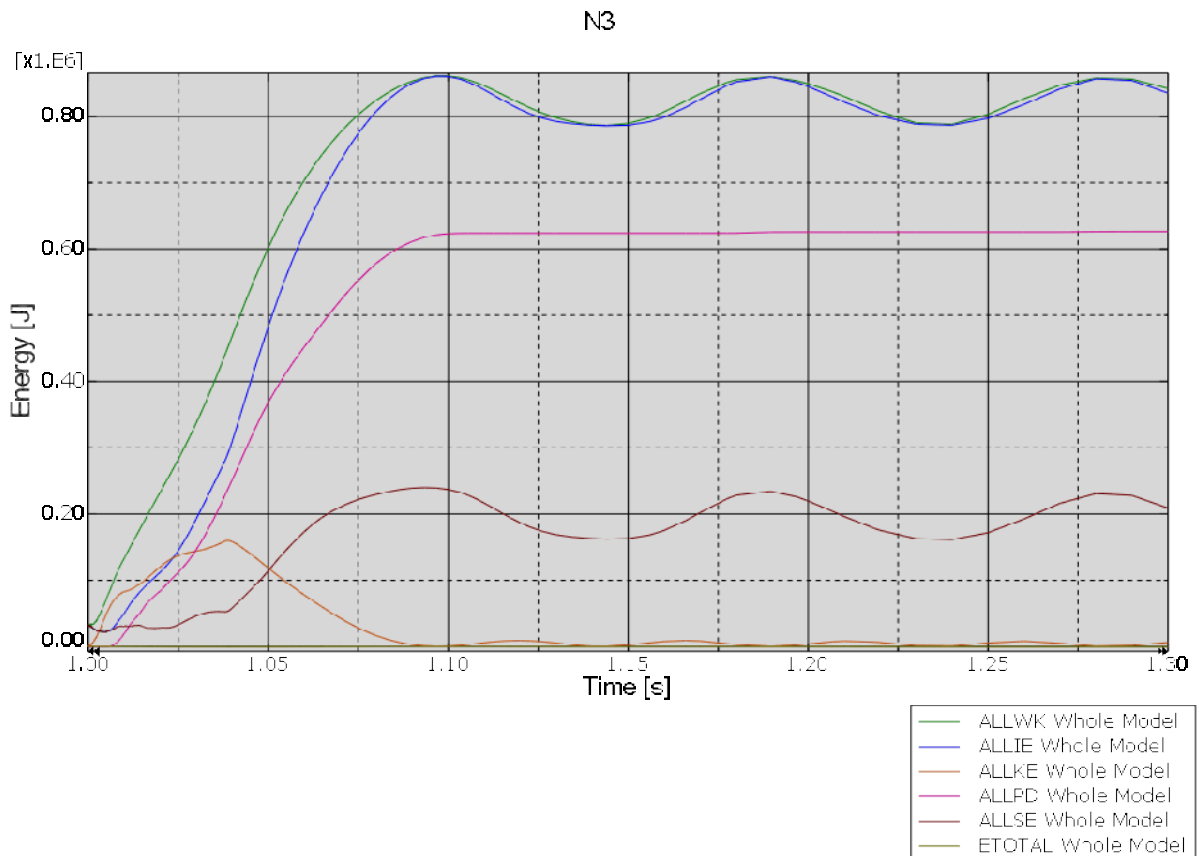


Figure 25. Energy balance (N3).

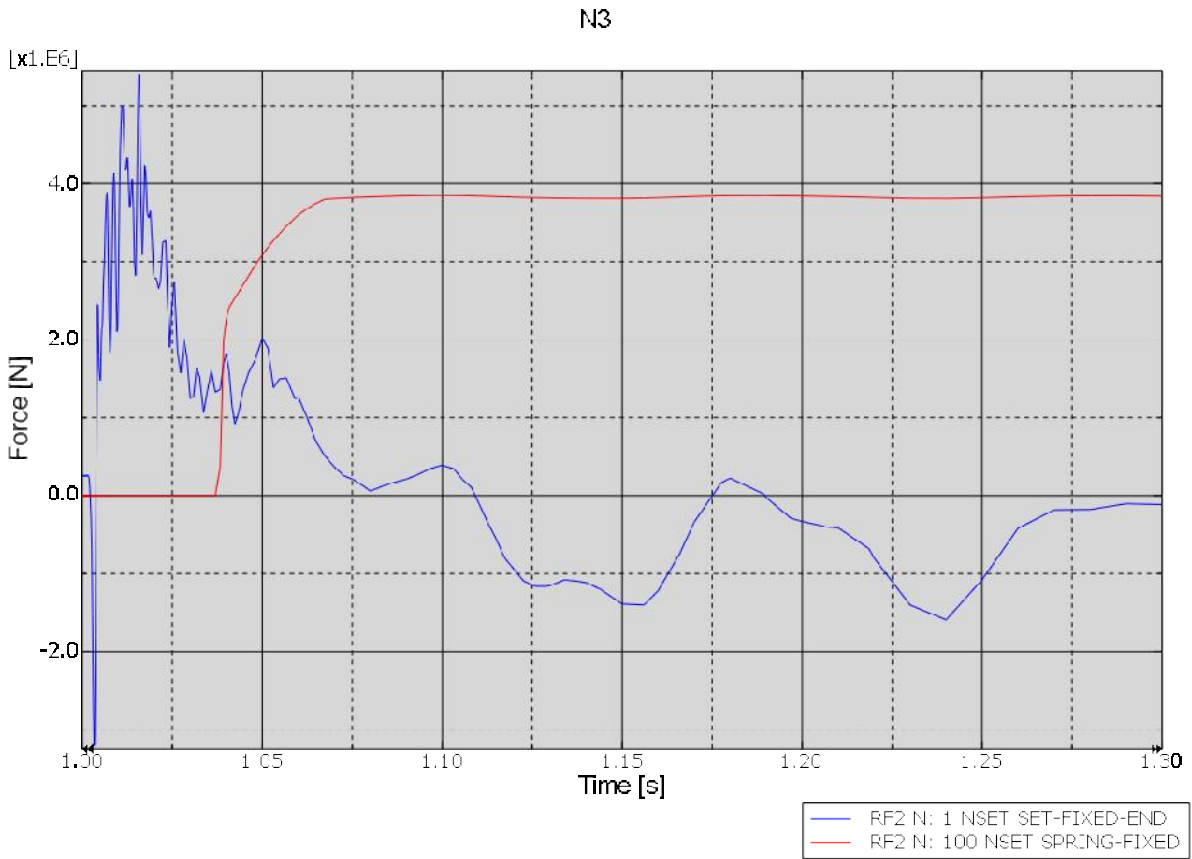


Figure 26. Vertical forces as functions of time in the right pipe end (blue) and in the fixed end of the type B spring (red) (N3).

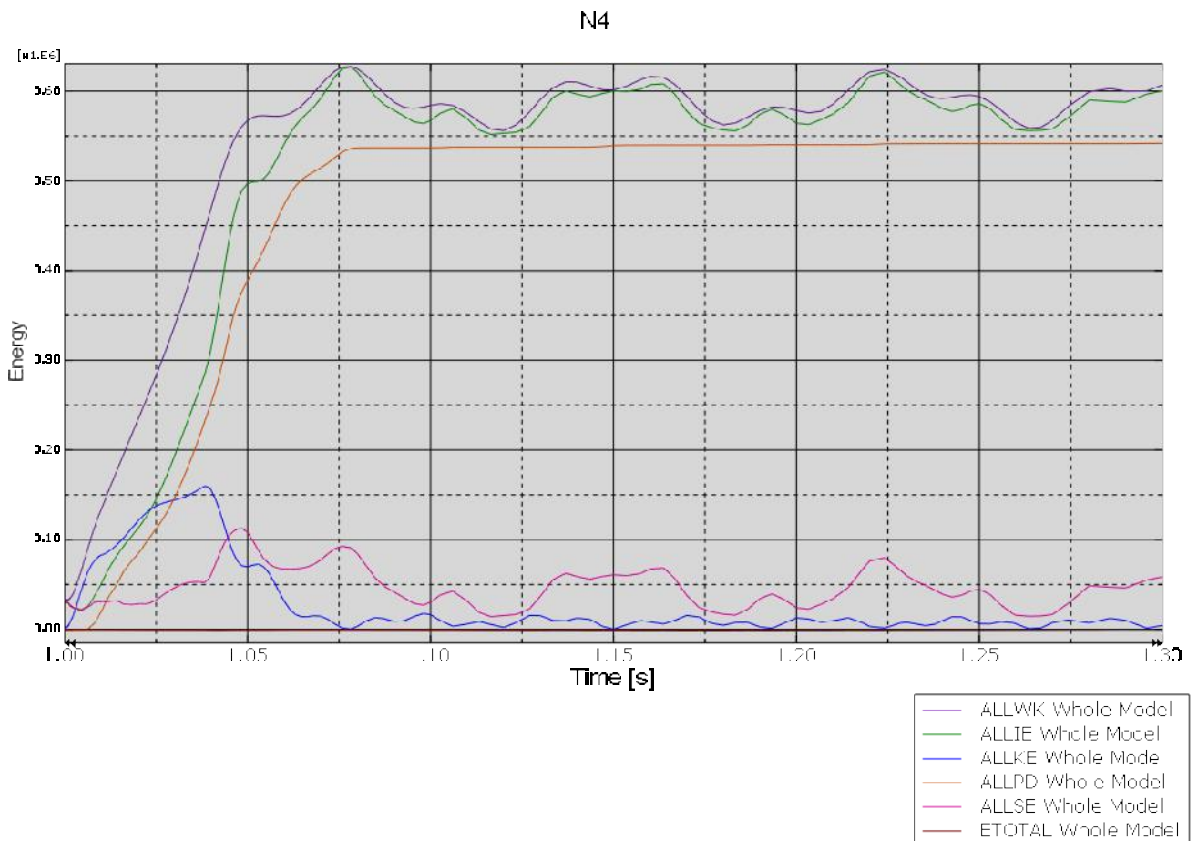


Figure 27. Energy balance (N4).

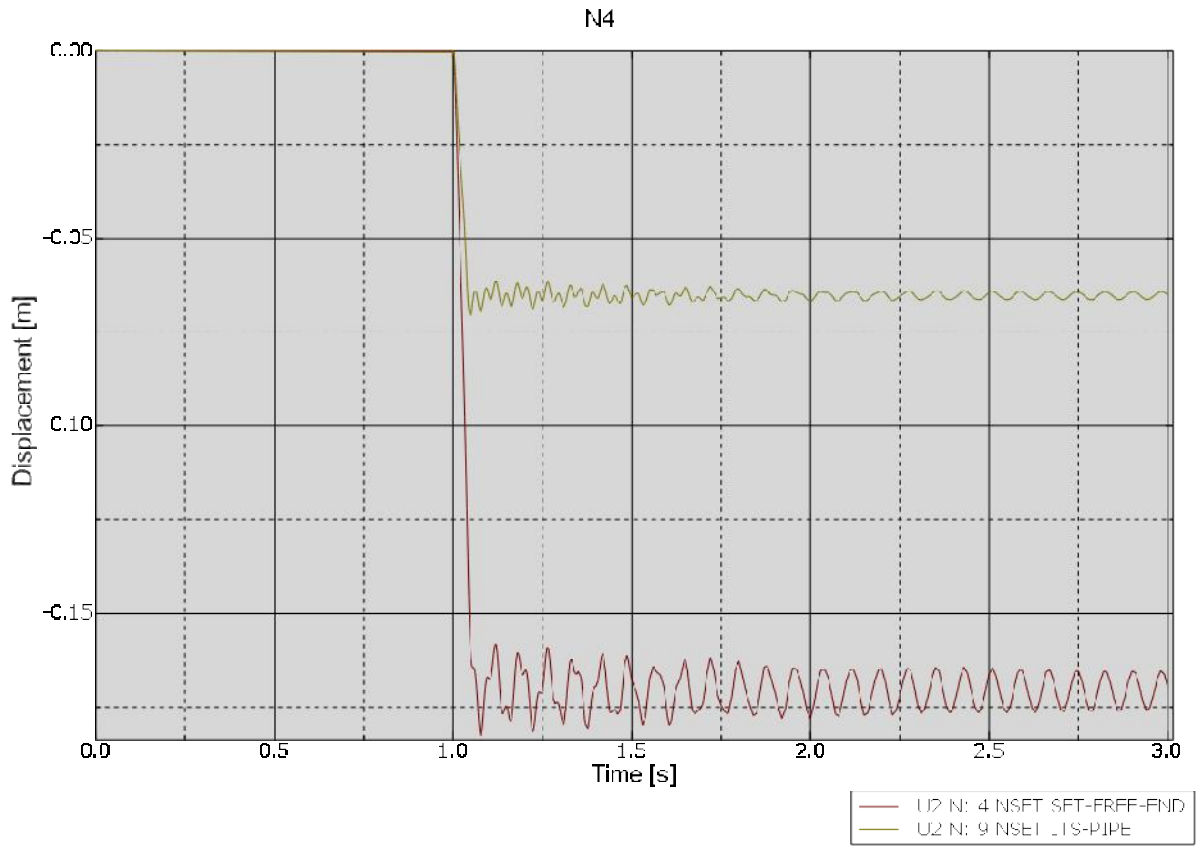


Figure 28. Vertical displacements of the free end (darker line) and of the pipe at the restraint (ITSUNI element) (N4).

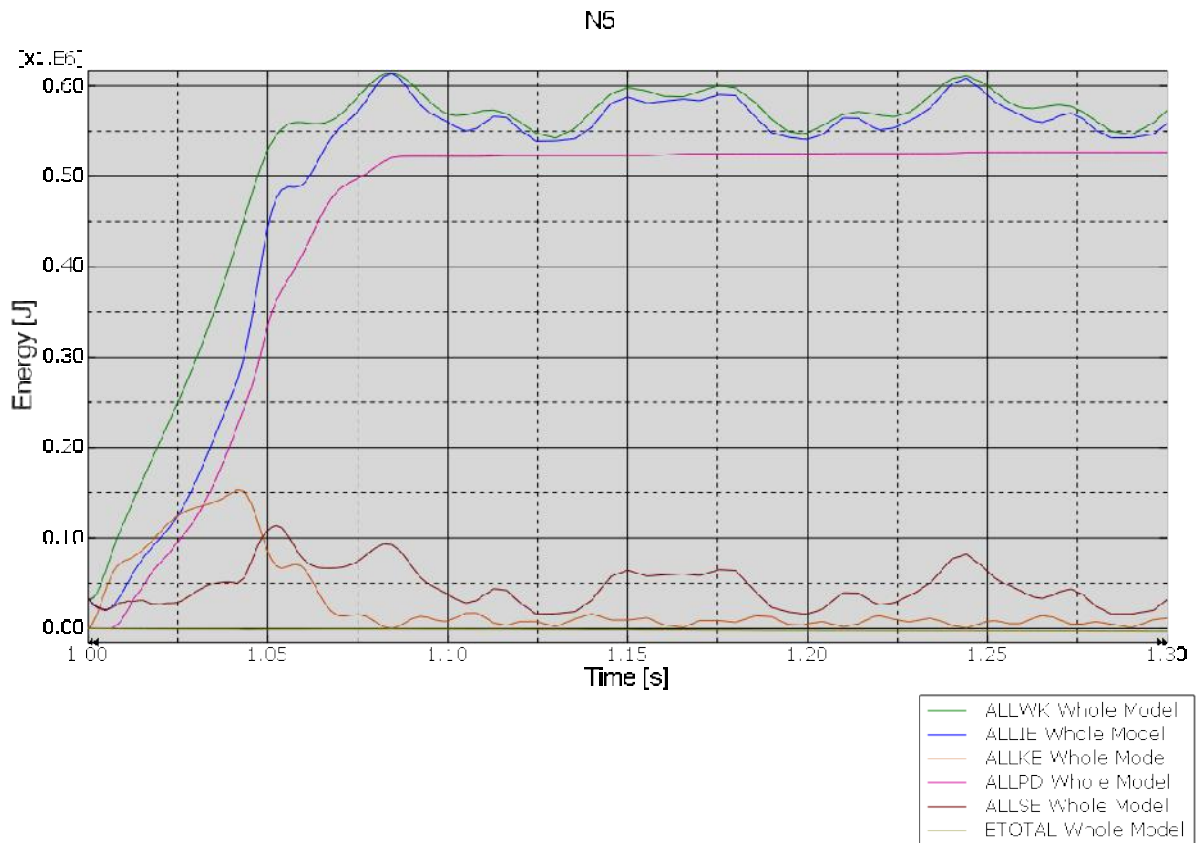


Figure 29. Energy balance (N5).

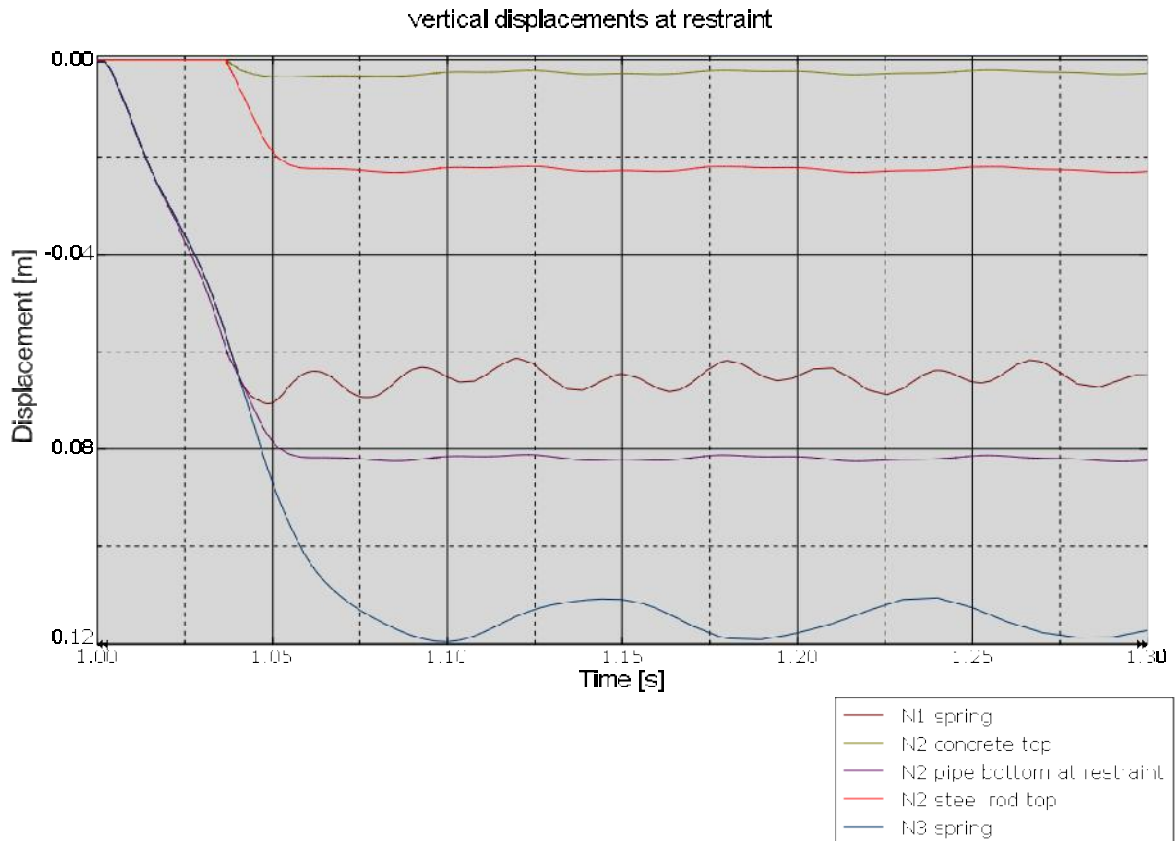


Figure 30. Vertical displacements of different locations at the restraint as functions of time in different cases (N1, N2 and N3).

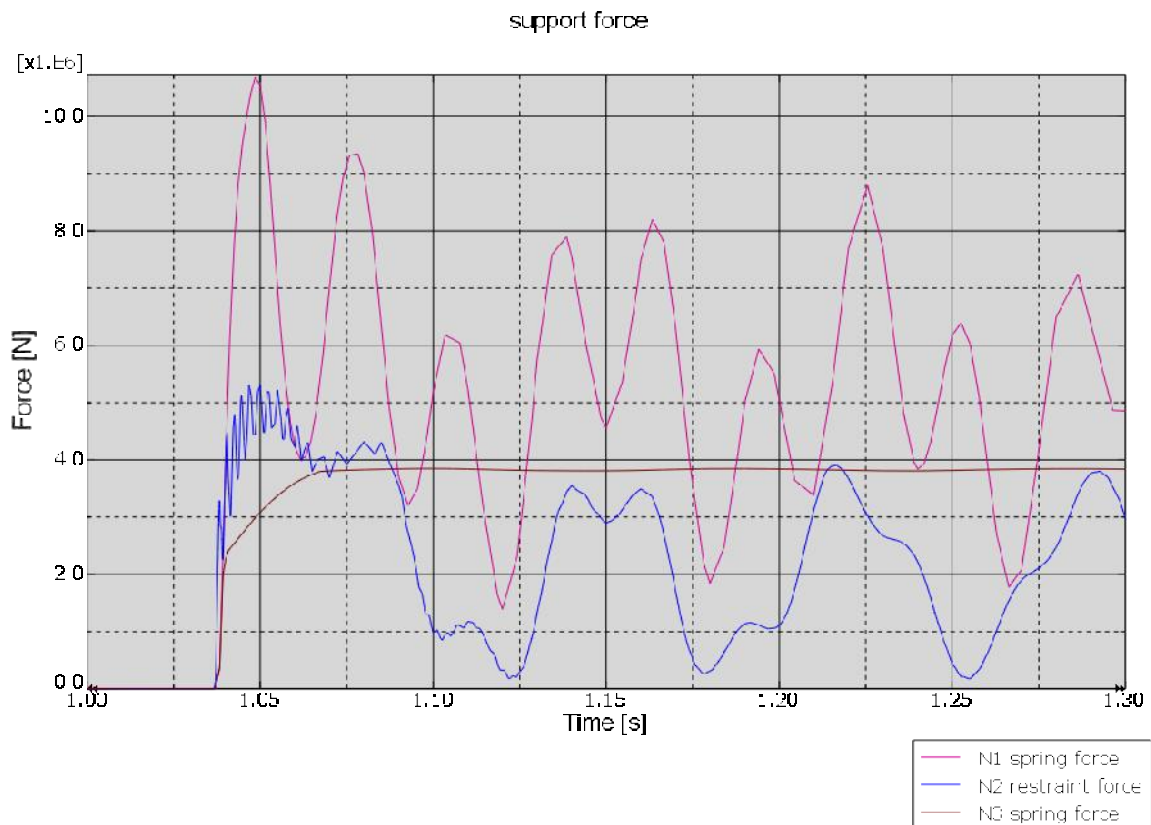


Figure 31. Vertical forces as functions of time in the restraint or spring in different cases (N1, N2 and N3).

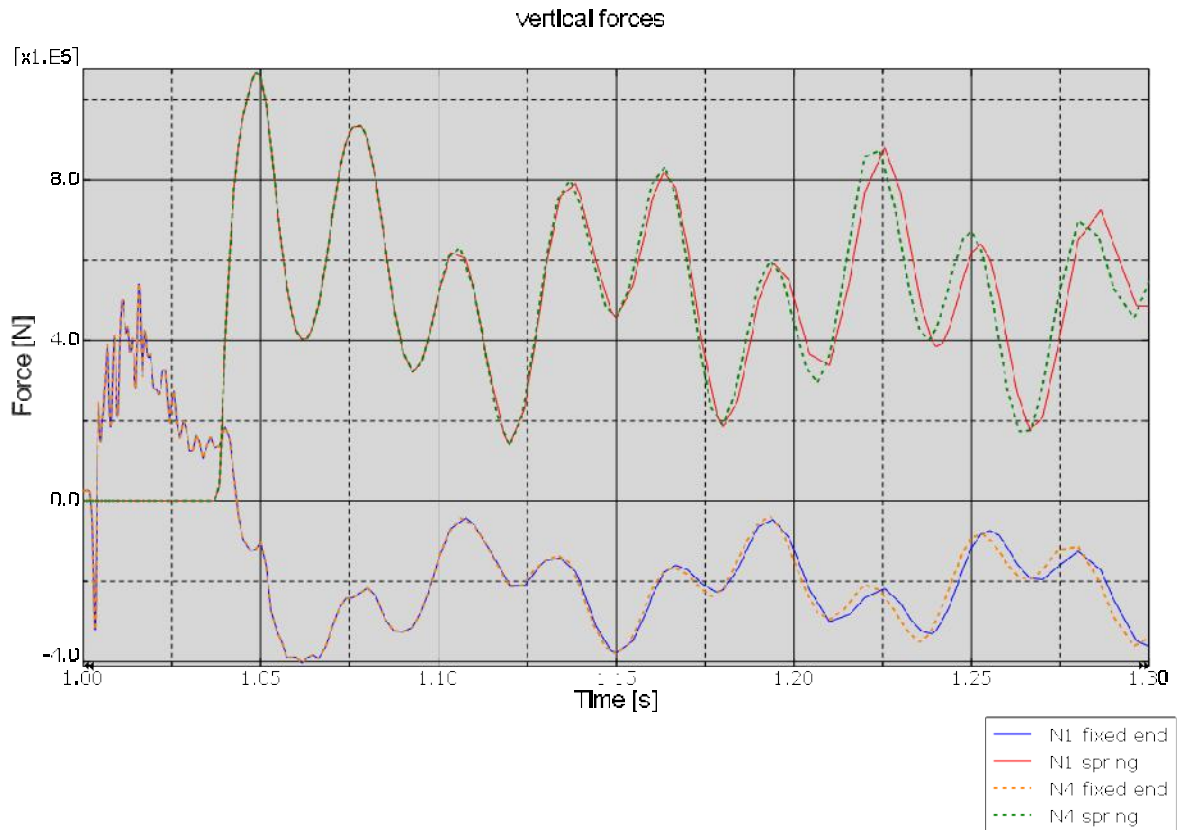


Figure 32. Vertical forces as functions of time in the right pipe end and in the fixed end of the type A spring (N1 and N4).

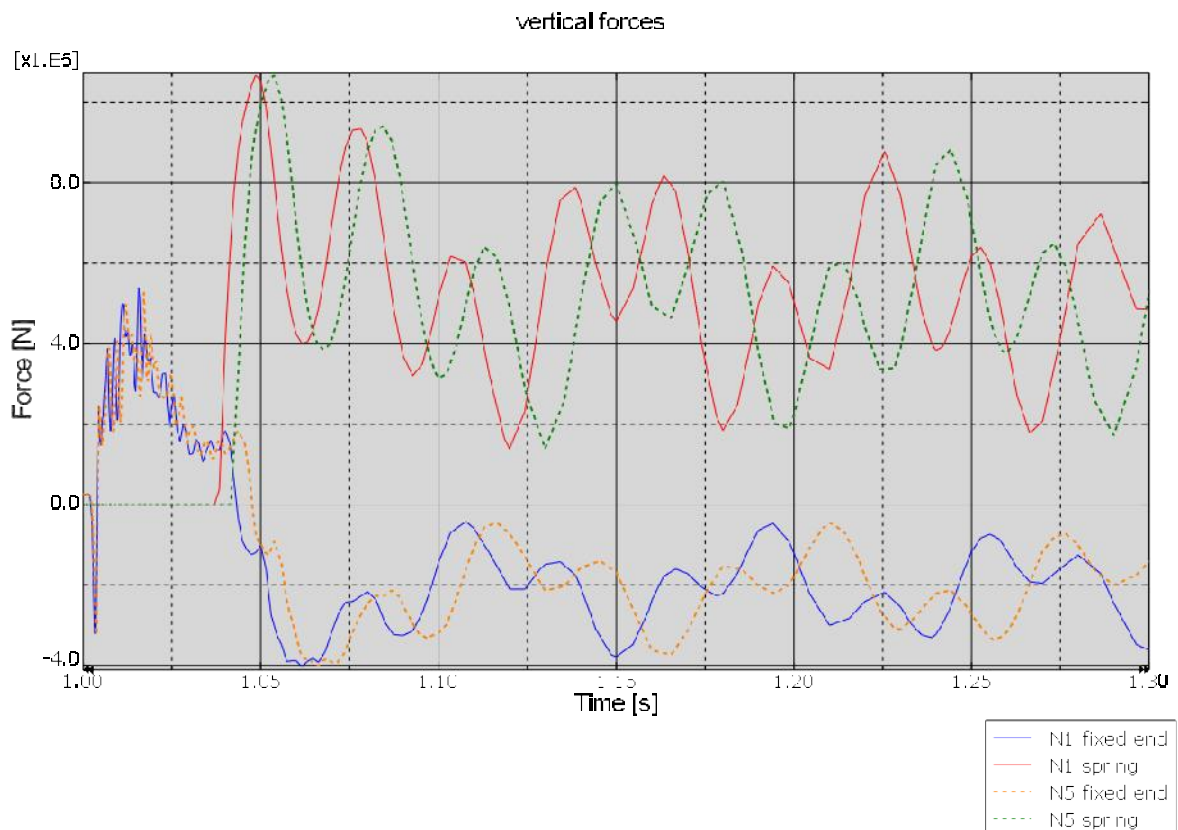


Figure 33. Vertical forces as functions of time in the right pipe end and in the fixed end of the type A spring (N1 and N5).

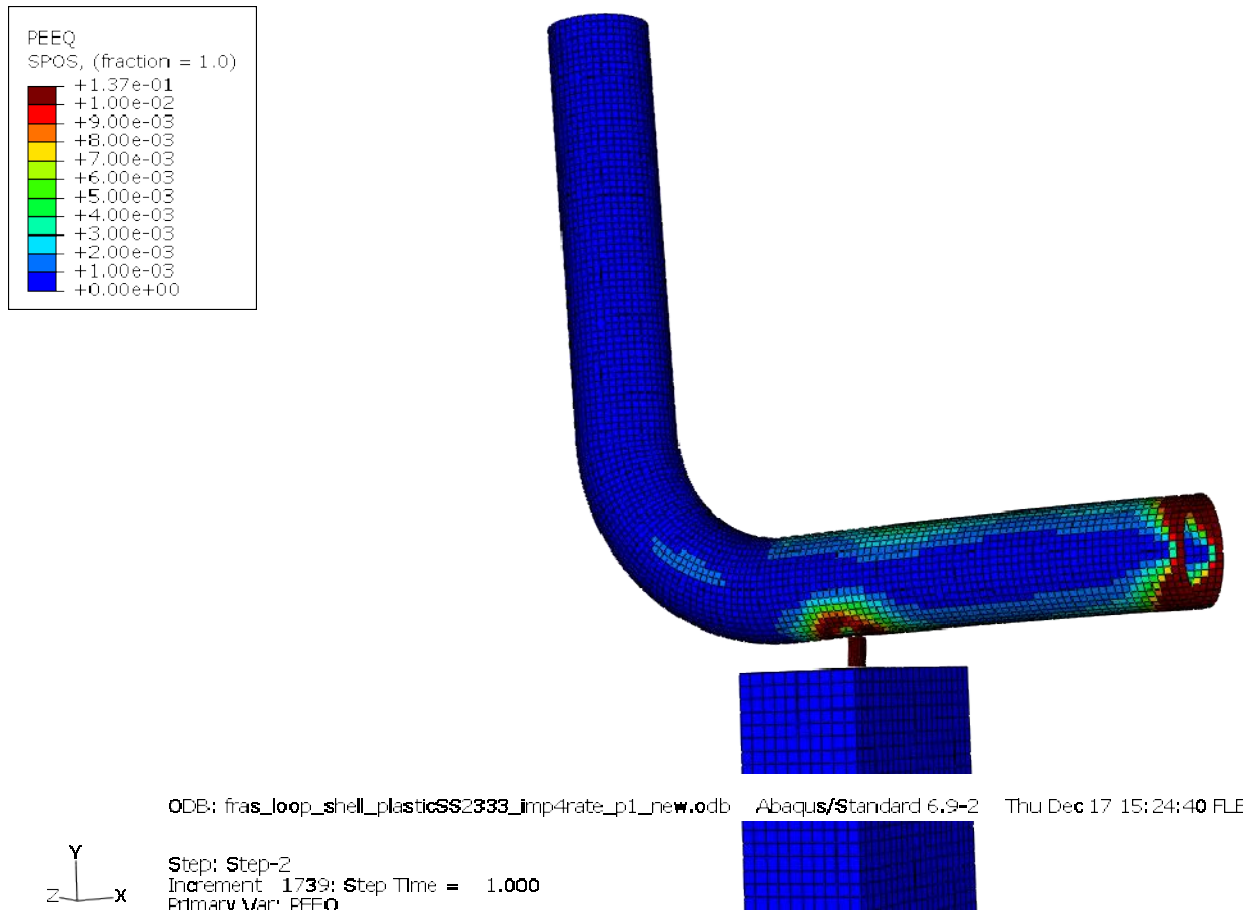


Figure 34. Equivalent plastic strain 1.0 seconds after the pipe break (N2). Values over 1% are in dark red colour.

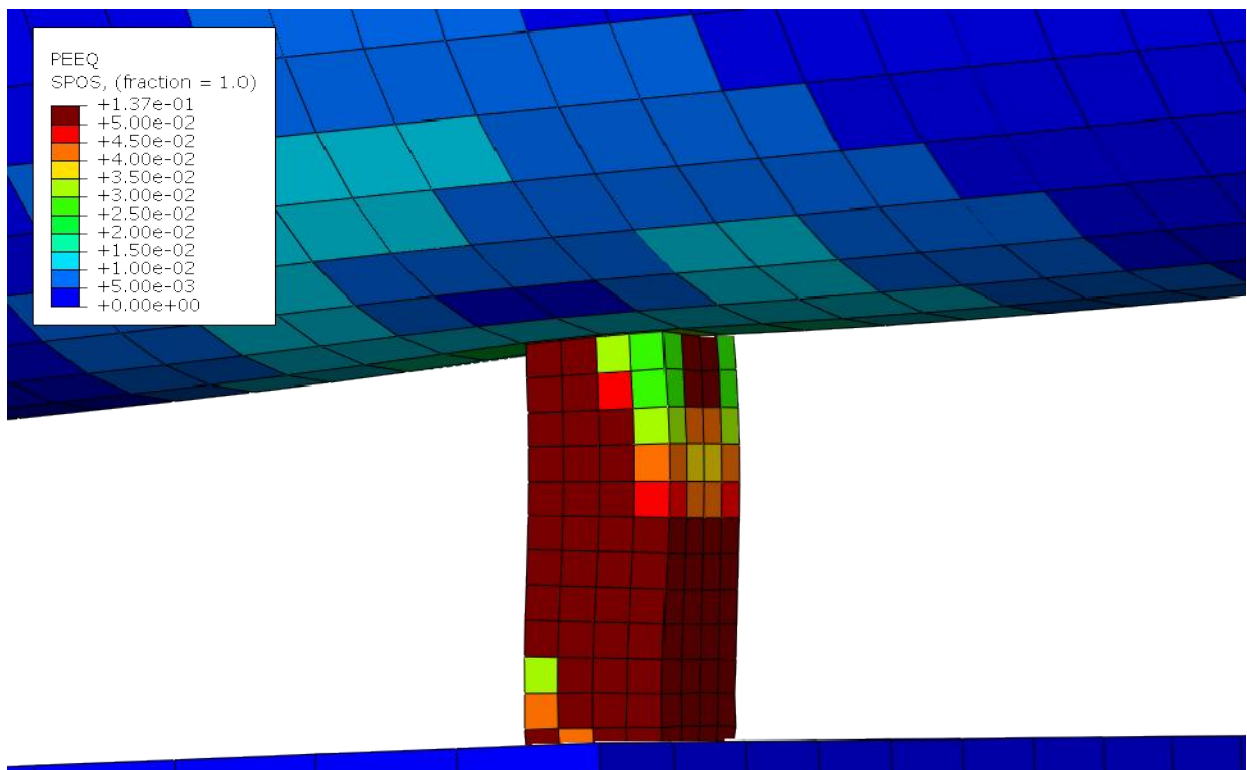


Figure 35. Equivalent plastic strain 1.0 seconds after the pipe break (N2). Values over 5% are in dark red colour.

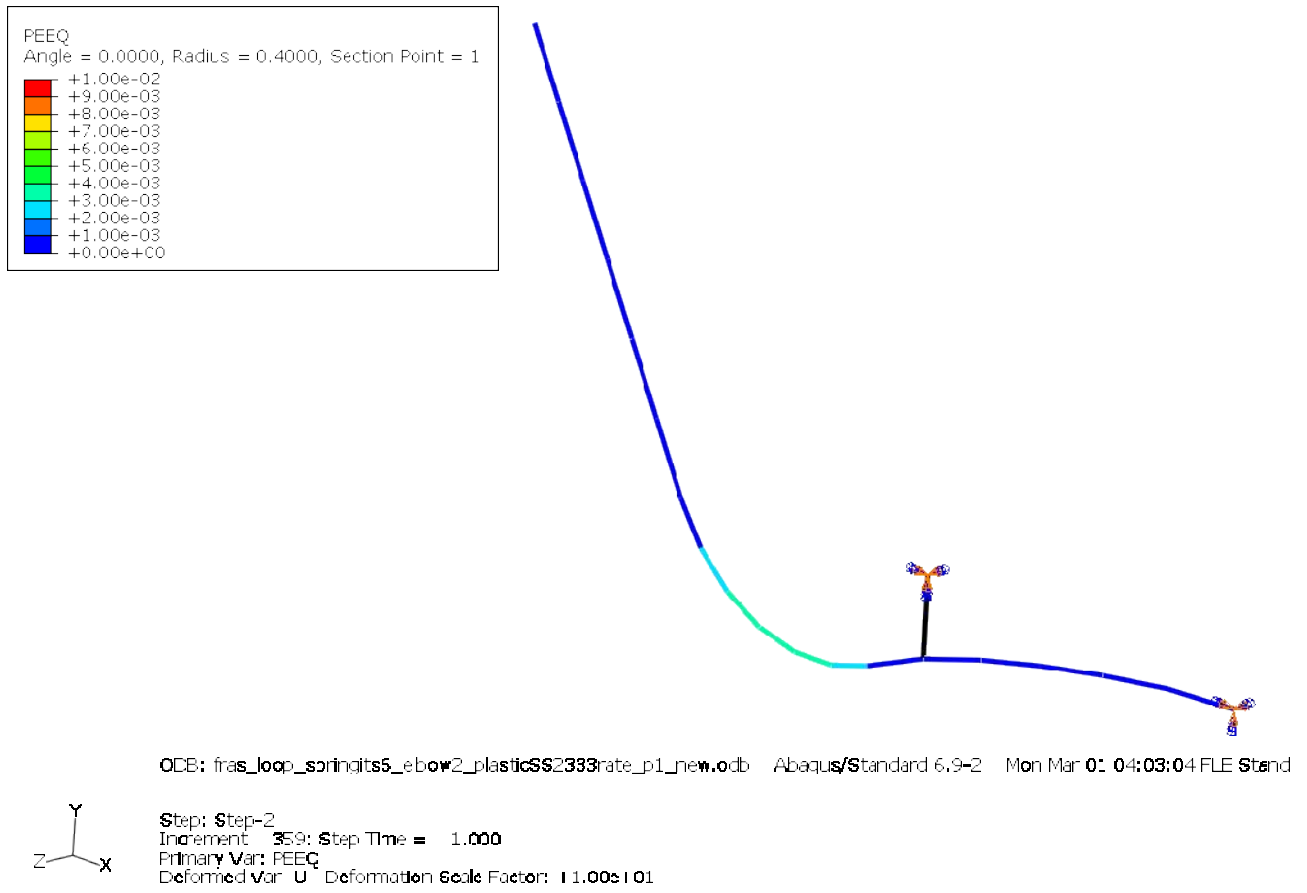


Figure 36. Equivalent plastic strain 1.0 seconds after the pipe break (N4). The pipe support element (ITSUNI) is shown in black. Deformations are scaled up by a factor of 10.

6 Dynamic analysis of an earthquake with new parameters

Dynamic analysis of an earthquake is conducted with the new model. It is not a sufficient structural design for earthquake resistance, but only a preliminary study concerning how to take the earthquake load into account. In a thorough assessment, one must first know the kind of shaking arriving to the base of the building and measure the shaking arriving to the location where the studied component (in this case the pipeline) is connected. This is possibly done together with some portion of the soil to have Soil-Structure interaction covered. In order to be able to complete that kind of assessment, as minimum one has to have the largest acceleration expected at the base of the building (PGA). The seismic source and its depth are the key factors for that. It would also be good to know something about the soil under the building. One must also have an evaluation of the fundamental vibration period of the building itself. The location of the pipe and the points it is fixed to in the building are also important. The dynamic properties of the nearest concrete wall are important because the wall works as a filter. It may increase some vibrations, while decreasing others at the same time (Fulop, 2009).

According to Eurocode 8, Part 1, (Eurocode, 2004) the earthquake motion at a given point on the surface is represented by an elastic ground acceleration response spectrum. Figure 37 shows recommended Type 1 elastic response spectra for ground types A to E with 5% damping. Usually, two different types (1 and 2) of spectra should be used. In the Y-axis, there is the elastic response spectrum divided (or normalised) by the design ground acceleration. The design ground acceleration is equal to the reference peak ground acceleration times the importance factor. In the X-axis, there is the vibration period of a linear single-degree-of-freedom system. Thus, in case of ground type A for instance, the vibration frequency of the peak spectra value ranges approximately from 3 Hz to 5 Hz.

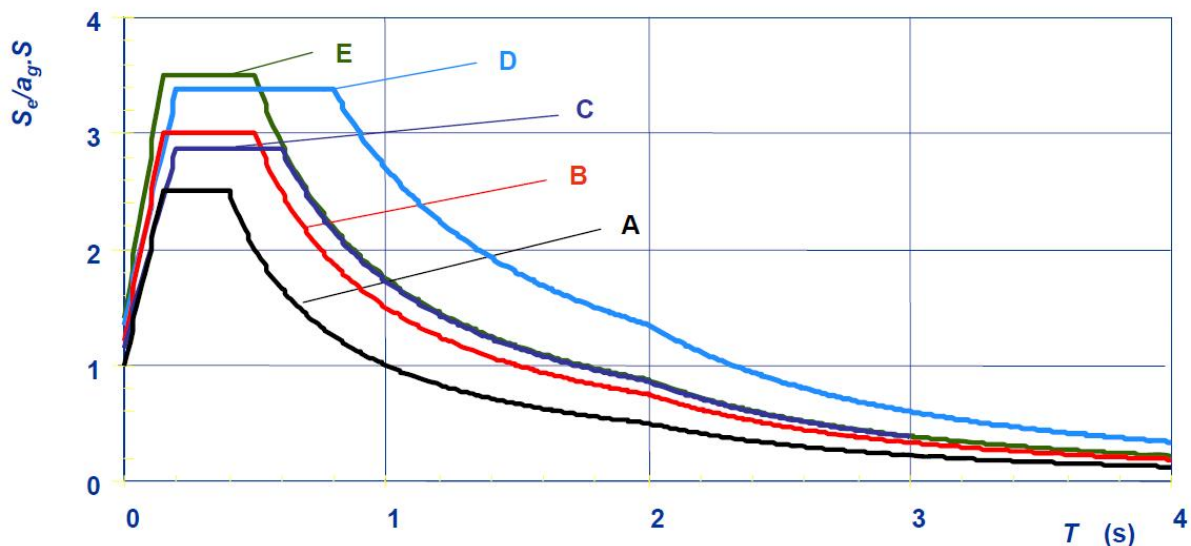


Figure 37. Recommended Type 1 elastic response spectra for ground types A to E with 5% damping (Eurocode, 2004).

Time-history representations of the earthquake motion may also be used. In this study, ground type A is used. It represents rock or other rock-like geological formation, including at most 5 m of weaker material at the surface. Figure 38 shows an artificial accelerogram generated from the type 1 spectra for ground type A (the black curve in Figure 37). It is used in the analysis as an excitation of the fixed end of the horizontal pipe section. It is scaled to a $PGA = 1 \text{ m/s}^2$ and to have a duration of 30 s. The accelerogram duration should be consistent with the magnitude and other relevant features of the seismic event underlying the establishment of the design ground acceleration. The minimum duration of the stationary part should be equal to 10 s, if no site-specific data are available. Figure 39 shows the first 5 seconds of the artificial earthquake signal used in the analysis.

Although officially a minimum of 3 different accelerograms should be used, only this one is used in this study. The two different cases are shown in Table 5. In case A1, the accelerogram shown in Figure 38 is used. In case A1 x 10, that signal is multiplied by 10, i.e. it is scaled up to a $PGA = 10 \text{ m/s}^2$. Excluding the load type and the pressure being constant, the model and analysis parameters correspond to the ones used in case N1 (see Table 4). The left end of the pipeline is fixed (in case N1 it was released at the instant of the assumed pipe break). The right end is otherwise fixed, but translational movement in z-direction, or in global 3-direction, or in the horizontal direction perpendicular to the pipe axis, is free. The accelerograms are used in the analyses as excitations of the fixed end of the horizontal pipe section in the above-mentioned z-direction. Unfortunately, it is not the direction of the restraint behaviour. Vertical accelerograms are normally also used, but they are slightly lower by magnitude. Before the earthquake load, the inner pressure is applied statically in 1.0 seconds. According to the Eurocode, accelerograms should be used also in other directions in nonlinear dynamic analyses (Eurocode, 2004).

Table 5. Earthquake analysis cases with the new pipe dimensions and pressure.

| Case | Element type | Material | Rate dependence | Pressure | Spring | Signal |
|---------|--------------|----------|-----------------|----------|--------|---------------------|
| A1 | Elbow | C | Yes | Constant | A | A-1 |
| A1 x 10 | Elbow | C | Yes | Constant | A | A-1 amplified by 10 |

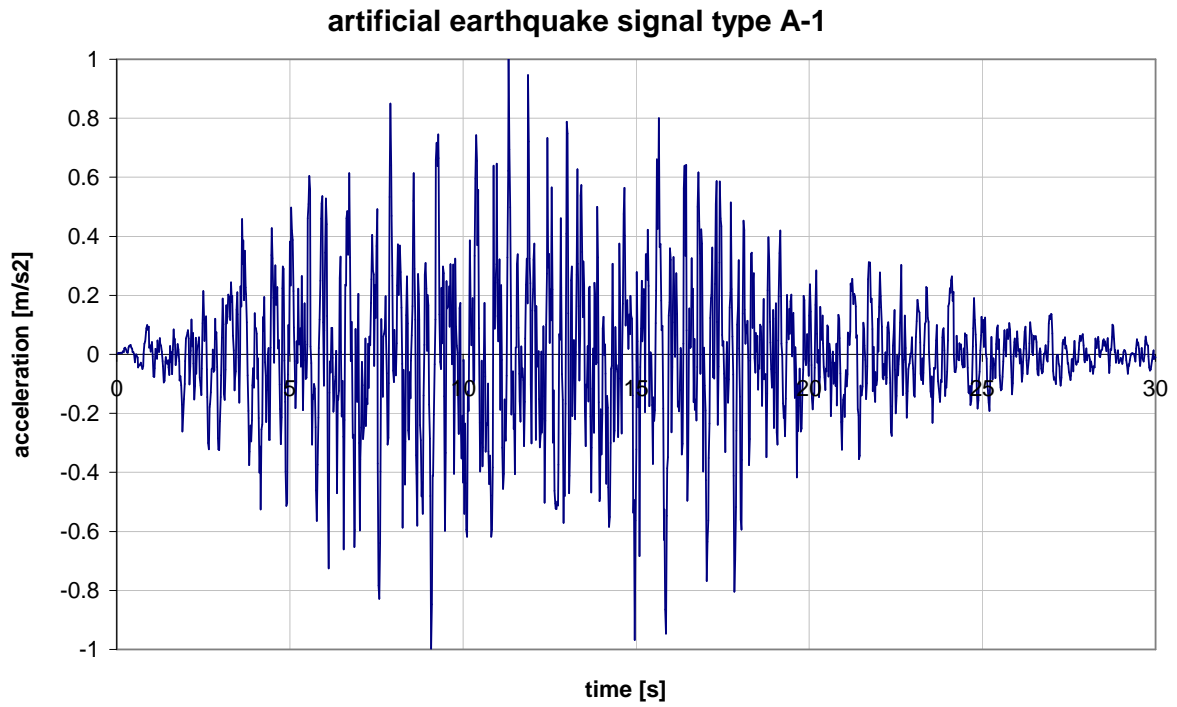


Figure 38. Artificial earthquake signal (accelerogram) used in the analysis.

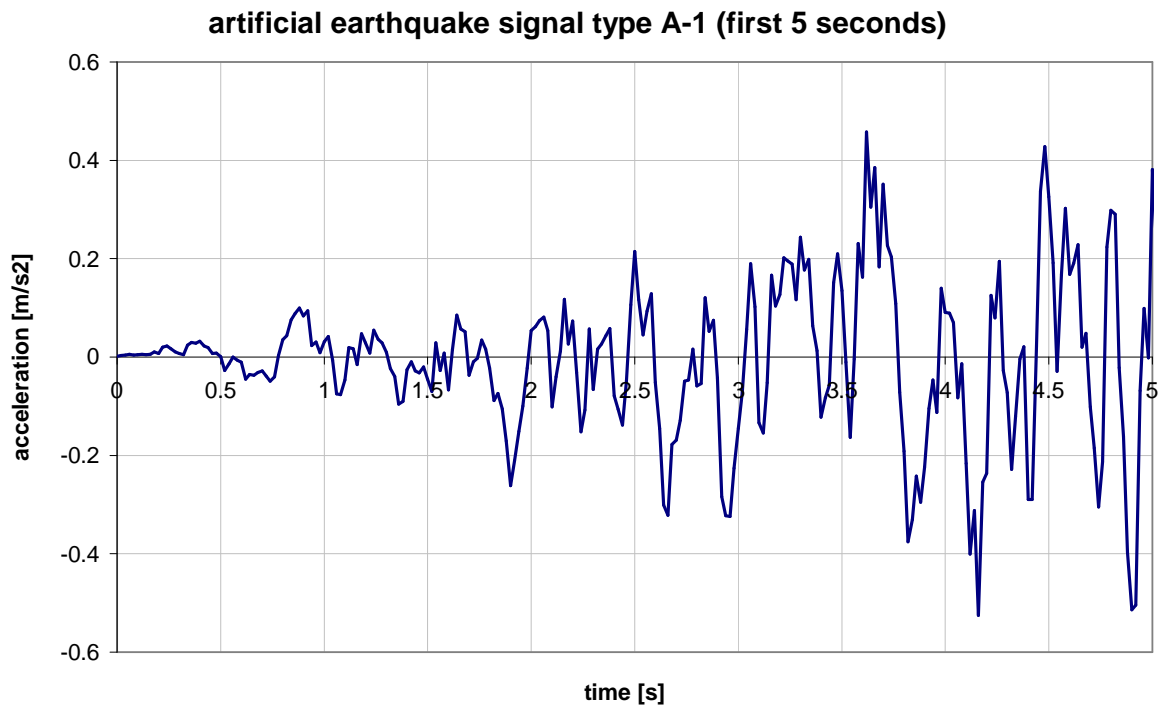


Figure 39. First 5 seconds of the artificial earthquake signal used in the analysis.

The analyses were conducted with Abaqus/Standard version 6.9-2. They require several thousands of time increments to capture the signal with all its peaks but with this kind of small model, the total CPU time is only few minutes.

Figure 40 shows the energy balance in case A1. It is maintained. Figure 41 shows the reaction forces in horizontal, global 1 direction, in different locations. Notice that it is the axial direction of the pipe, not the direction of the excitation. Figure 42 shows the reaction forces in vertical, global 2 direction, in different locations. The pipe obviously does not hit the restraint. Figure 43 shows the reaction force in horizontal, global 3 direction, which is the excitation direction. The maximum reaction force in both ends is approximately 2.3 MN in both positive and negative direction. The pipe acts very stiffly since the forces are very similar in both ends.

Figure 44 shows the acceleration in global 3 direction in the excited end (blue curve) and in the spring (orange curve) in case A1. The blue curve corresponds to the applied acceleration as it should. The orange curve is very similar. The large peak is due to the start of the dynamic step with the high inner pressure. Figure 45 shows the corresponding displacements. The maximum displacement of the right end of the pipe is 6 cm. Now, the situation is unrealistic, since the “residual” displacement after the earthquake load is not zero but 2 cm, which is notably large for the whole power plant. This is due to the numerical error in integration of the acceleration, or mainly due to a minimal inaccuracy in the accelerogram. This kind of error should be avoided. The accelerogram can be modified to give zero displacement or the displacement history integrated from the accelerogram and modified having zero residual displacement can be used as an excitation.

Figure 46 shows the energy balance in case A1 x 10. It is maintained. The maximum energy value of the system is 90 times higher than the one in the case with 10 times lower accelerations. Figure 47 shows the reaction forces in horizontal, global 1 direction, in different locations. Notice that it is the axial direction of the pipe, not the direction of the excitation. Figure 48 shows the reaction forces in vertical, global 2 direction, in different locations. The pipe obviously hits the restraint. Figure 49 shows the reaction force in horizontal, global 3 direction, which is the excitation direction. The maximum reaction force in the right end is approximately 11.5 MN in both positive and negative direction. The forces are slightly lower in the left end. Now, the spring element acts also in this direction since SPRINGA element acts between two nodes, with its line of action being the line joining the two nodes, so that this line of action can rotate in a large-displacement analysis. It is not very realistic considering the pipe-restraint structure where the small restraint tip practically takes only loads in one fixed direction. In that sense, SPRING1 or SPRING2 would have been better choices for the restraint. SPRING1 is between a node and ground, acting in a fixed direction. SPRING2 is between two nodes, acting in a fixed direction. SPRING1 and SPRING2 elements are available only in Abaqus/Standard.

Figure 50 shows the acceleration in global 3 direction in the excited end (blue curve) and in the spring (orange curve) in case A1 x 10. Figure 51 shows the corresponding displacements. The maximum displacement of the right end of the pipe is 60 cm. Now, the situation is even more unrealistic than in case A1, since the residual displacement after the earthquake load is not zero but 17 cm.

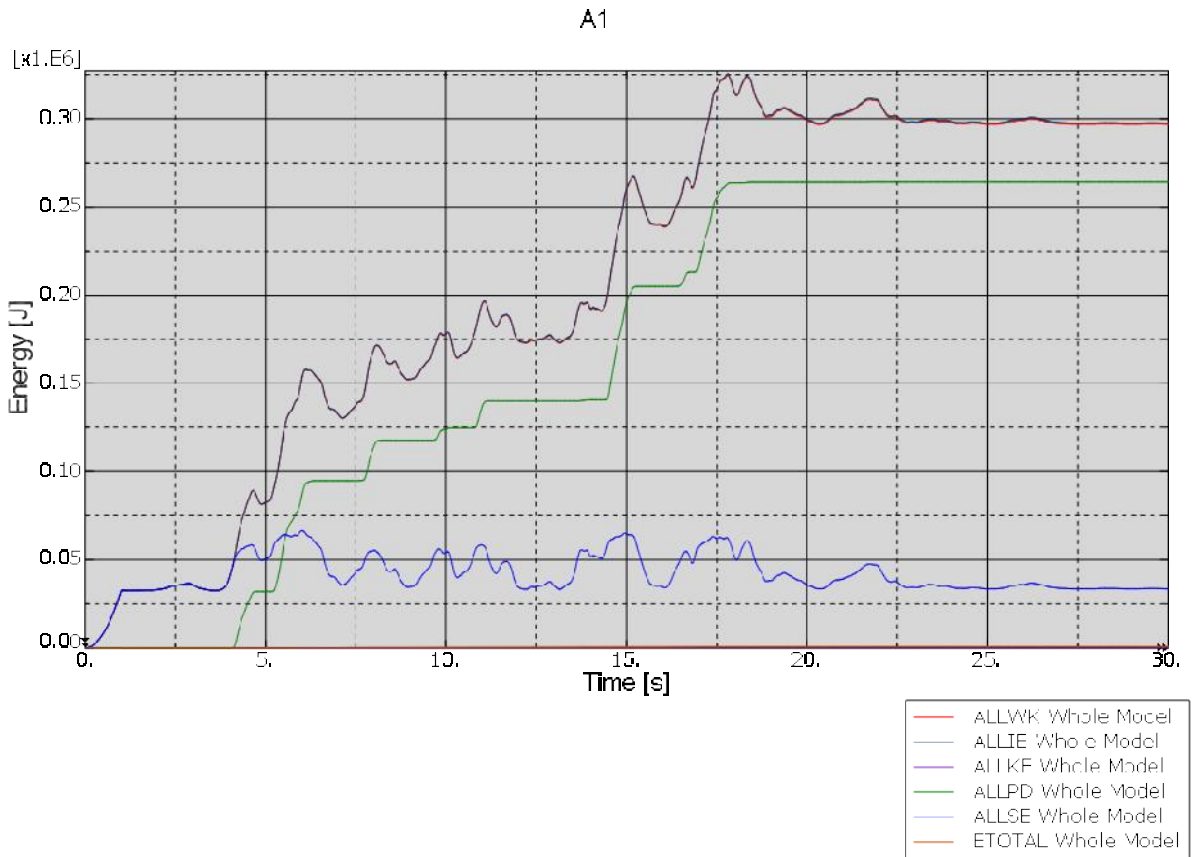


Figure 40. Energy balance (A1).

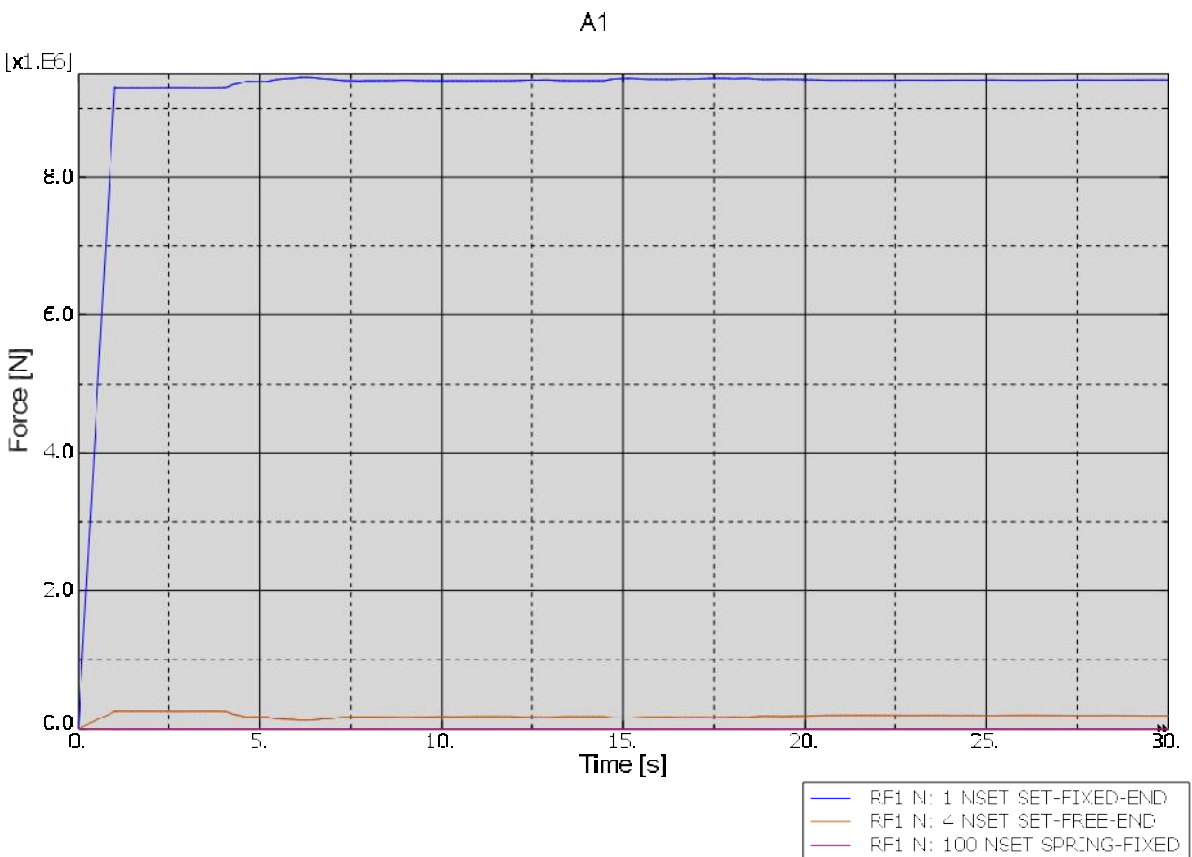


Figure 41. Reaction force in horizontal, global 1 direction (A1).

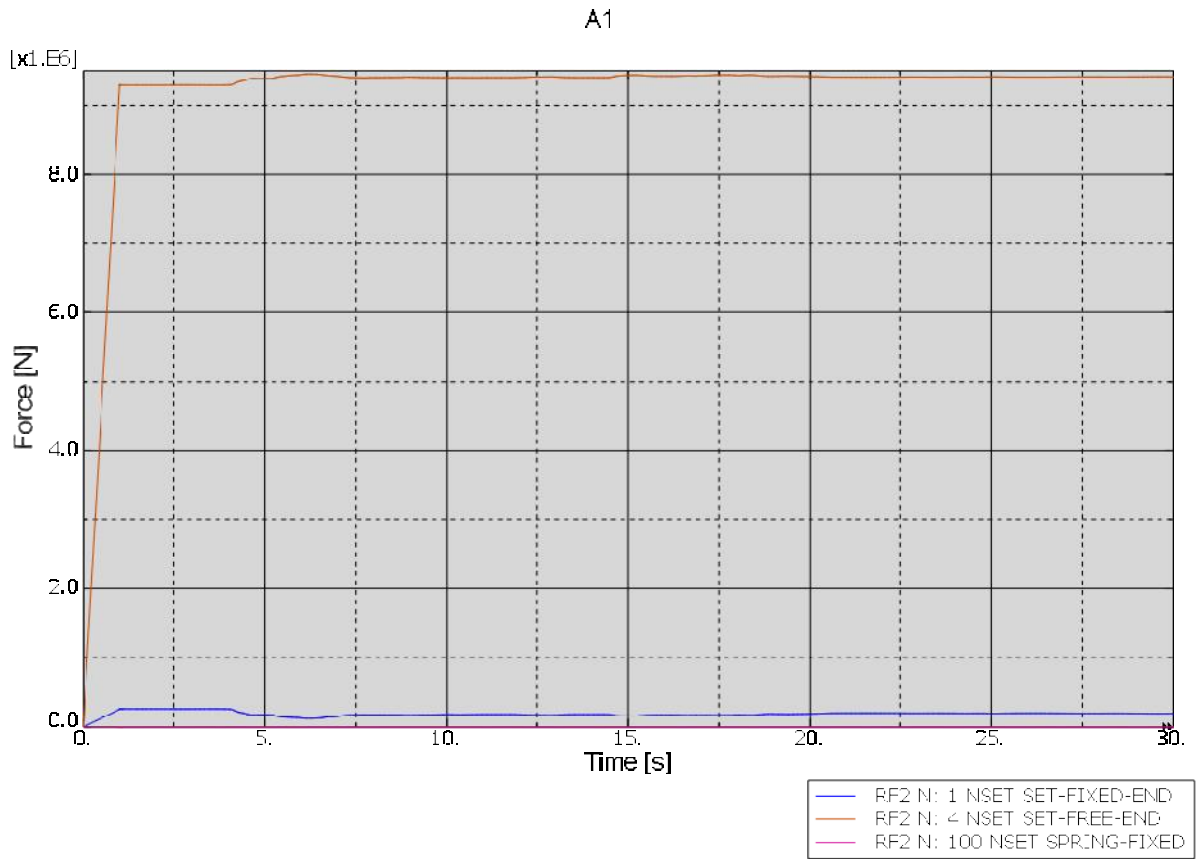


Figure 42. Reaction force in vertical, global 2 direction (A1).

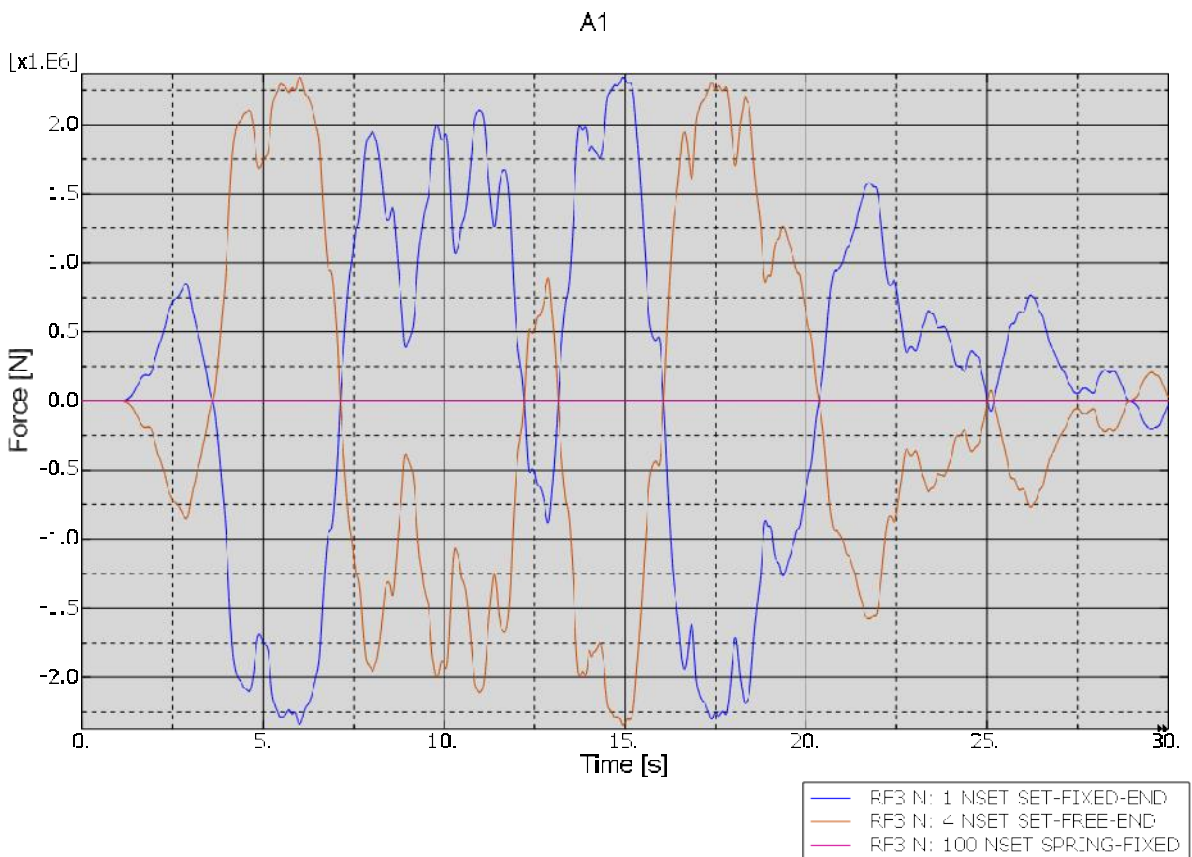


Figure 43. Reaction force in horizontal, global 3 direction (A1).

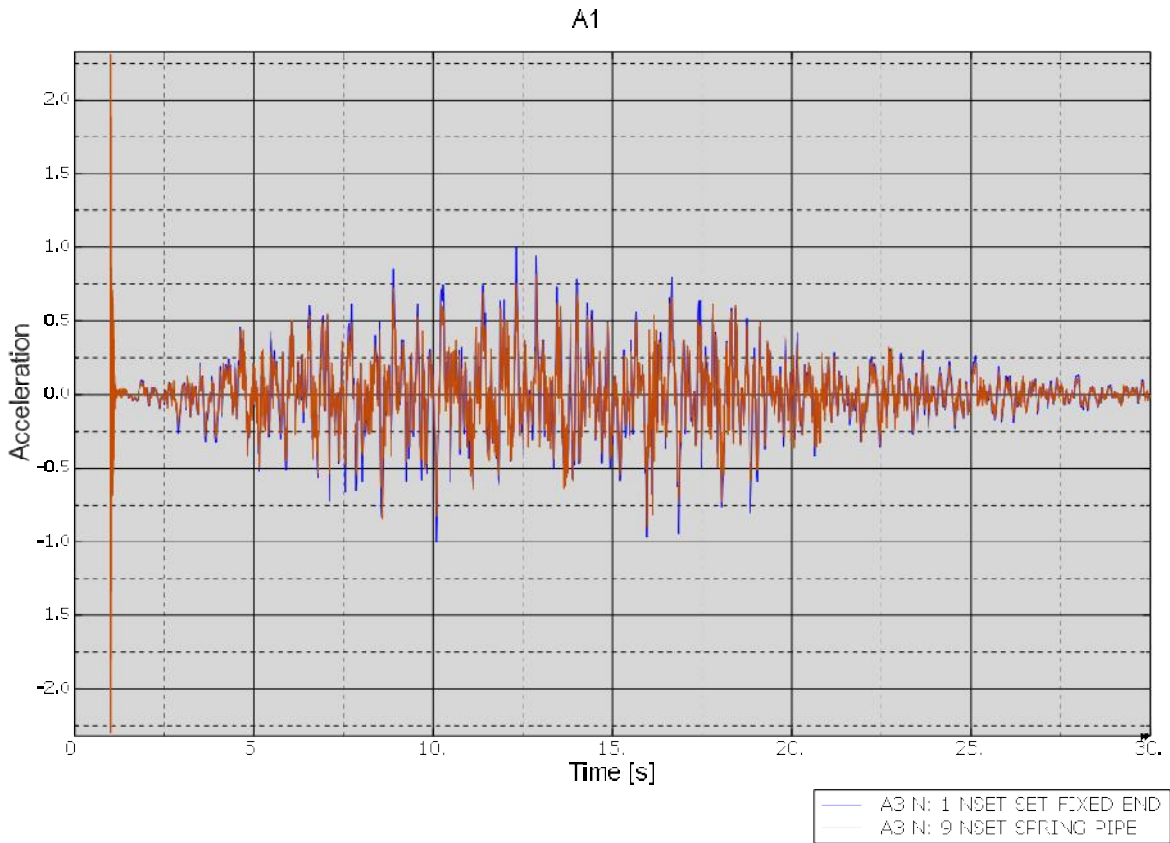


Figure 44. Acceleration in global 3 direction (A1).

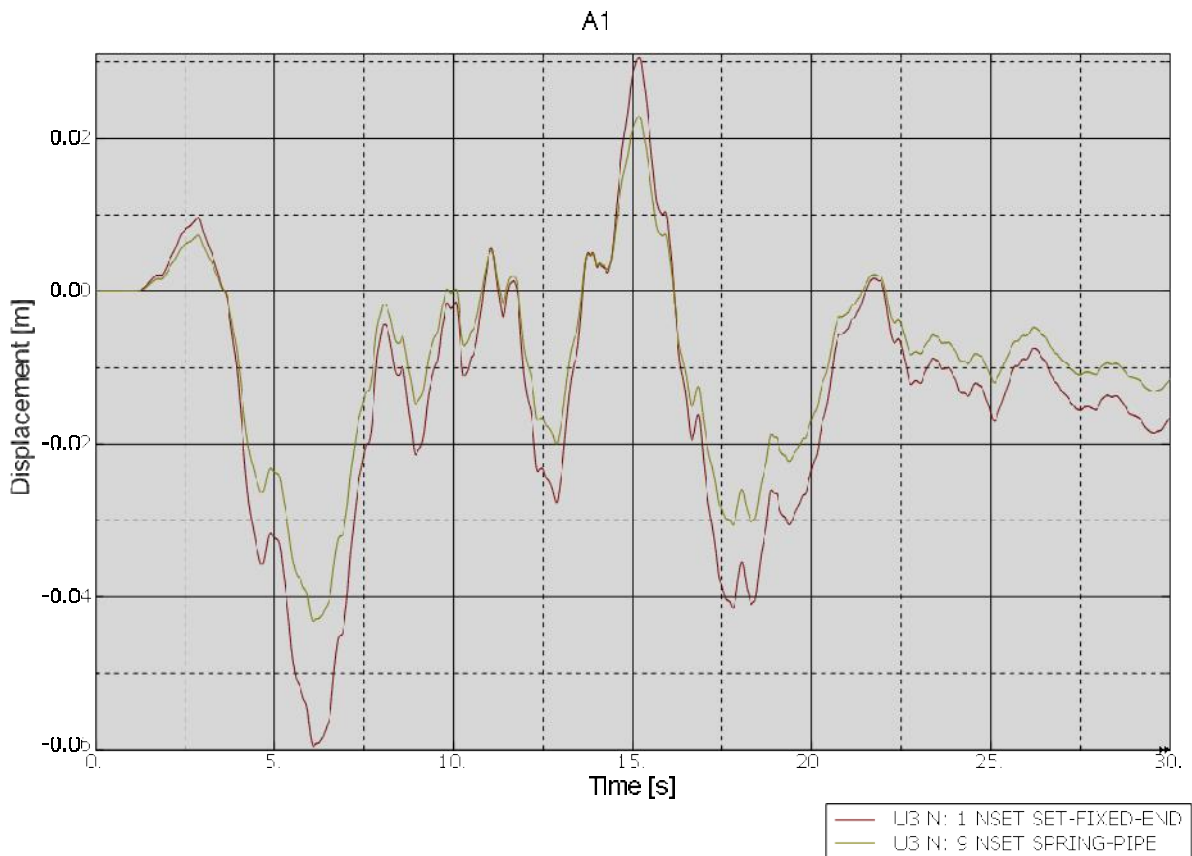


Figure 45. Displacement of the pipe in global 3 direction in the fixed end and at the spring (A1).

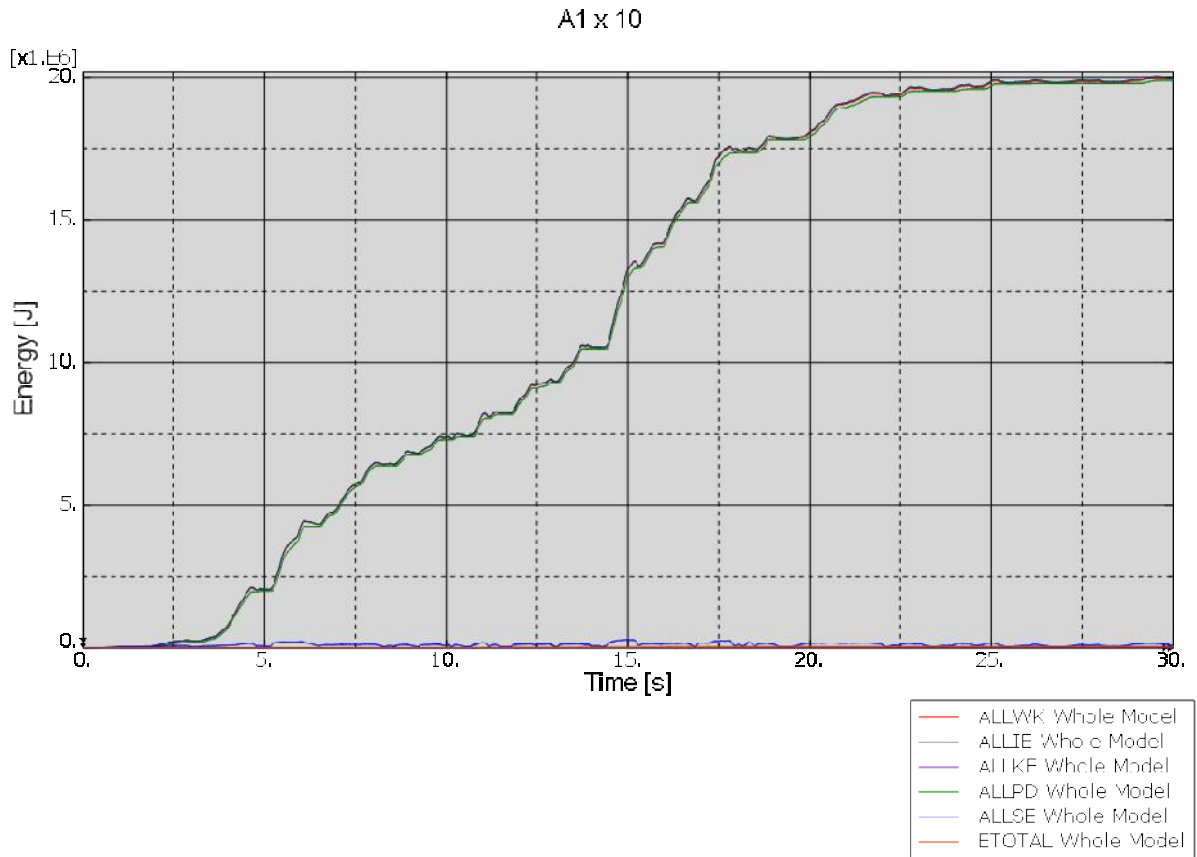


Figure 46. Energy balance (A1 x 10).

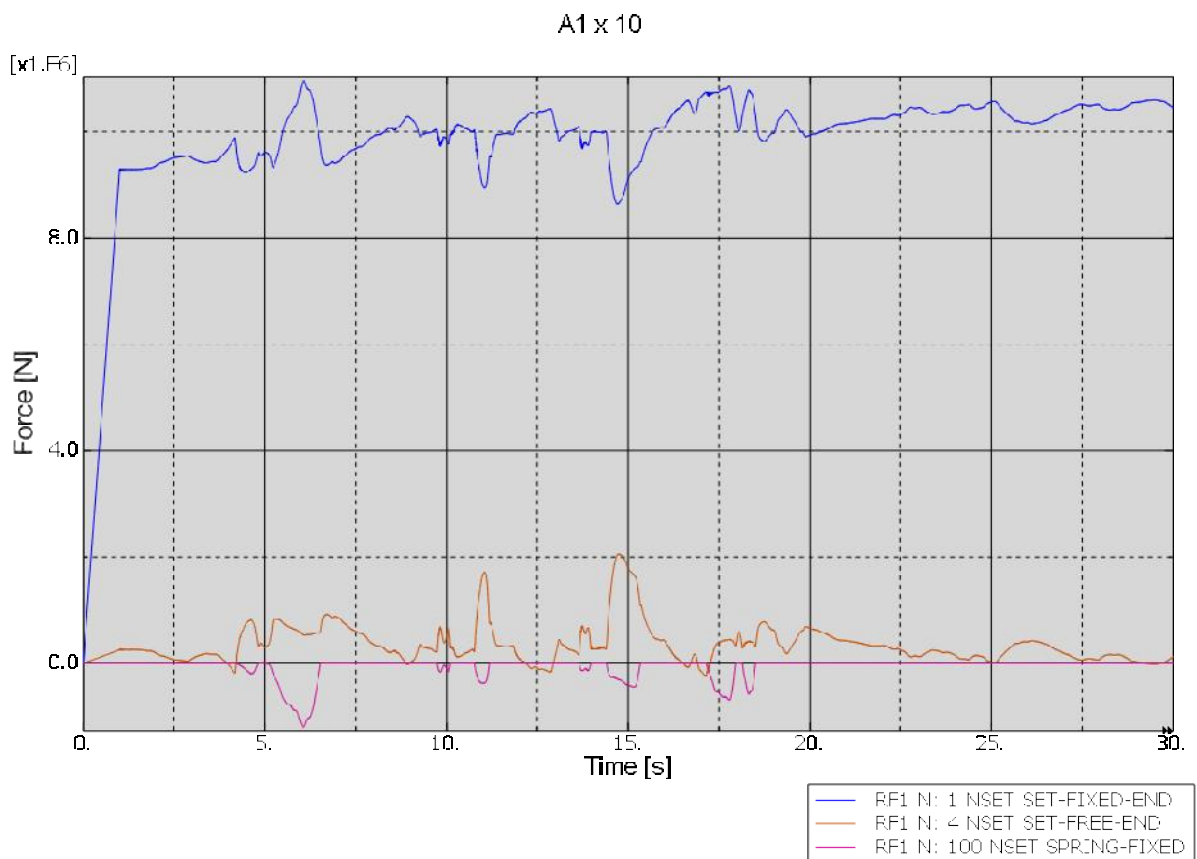


Figure 47. Reaction force in horizontal, global 1 direction (A1x10).

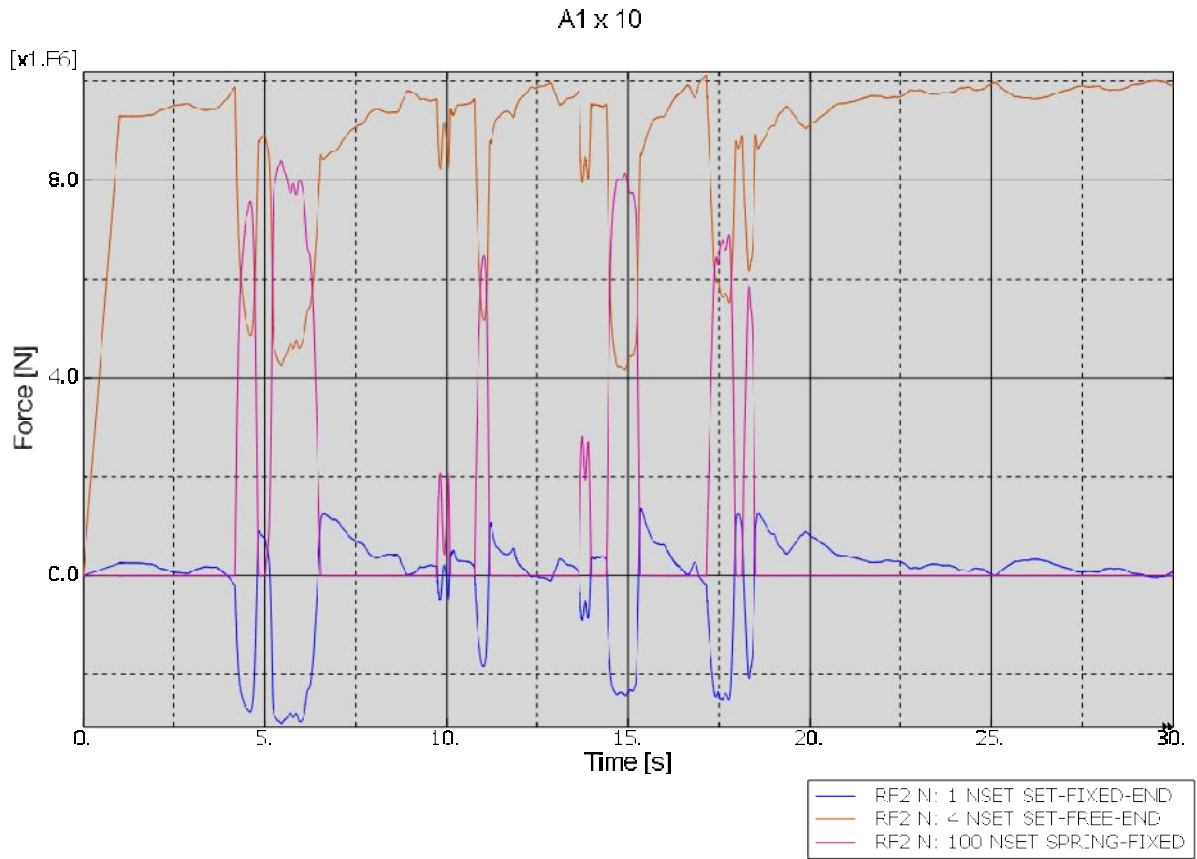


Figure 48. Reaction force in vertical, global 2 direction (A1x10).

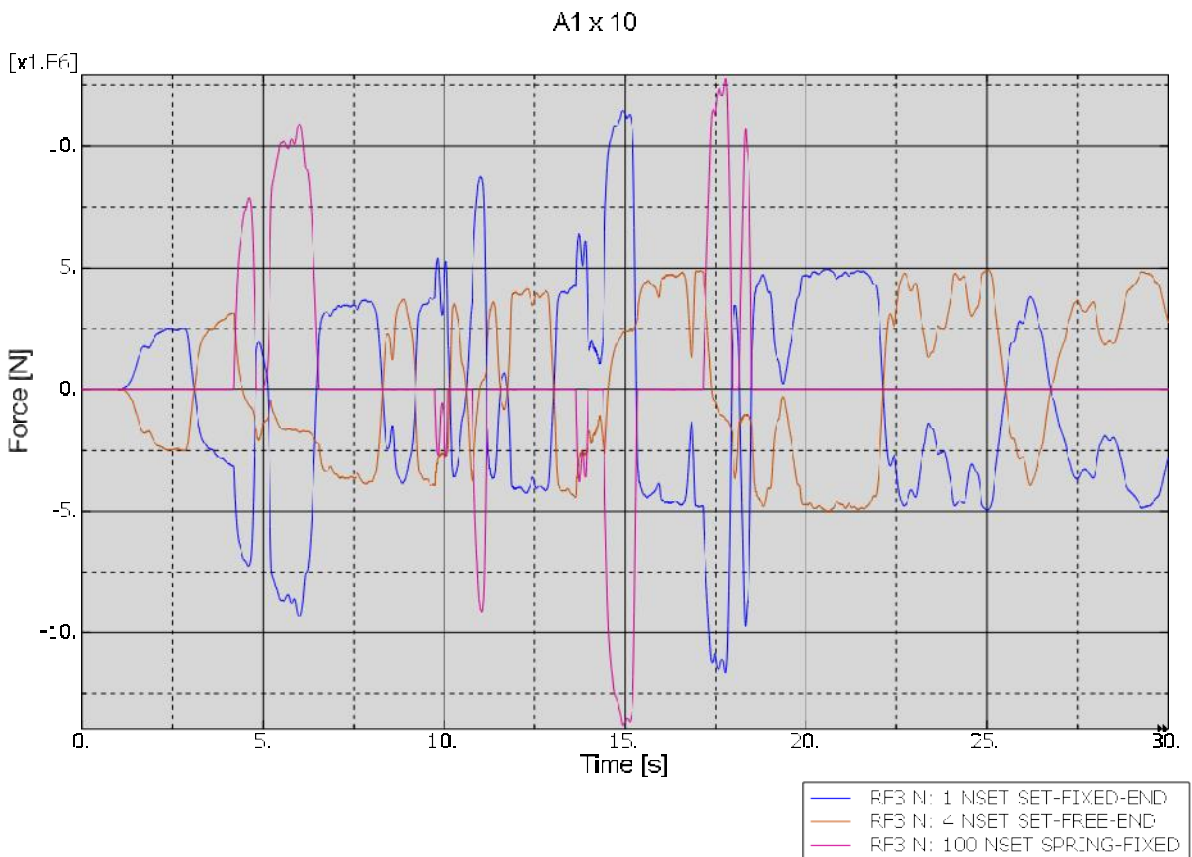


Figure 49. Reaction force in horizontal, global 3 direction (A1x10).

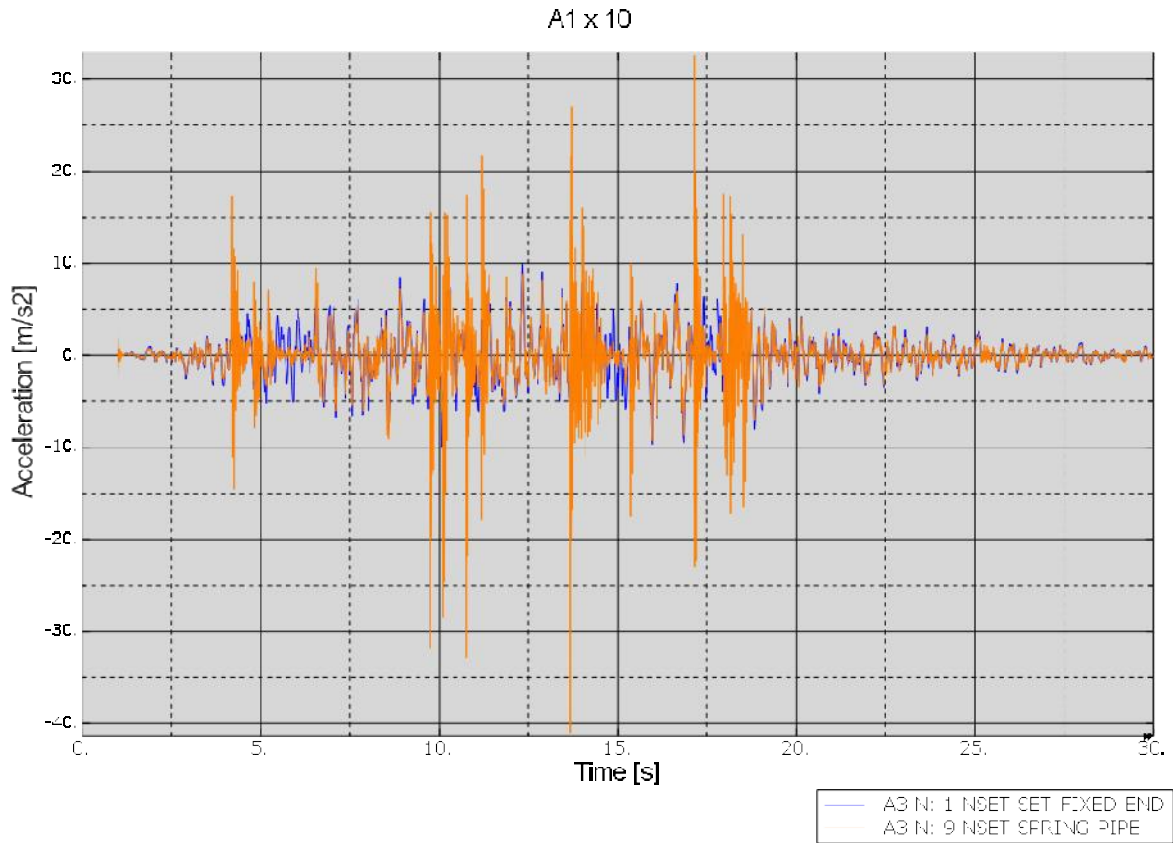


Figure 50. Acceleration in global 3 direction (A1x10).

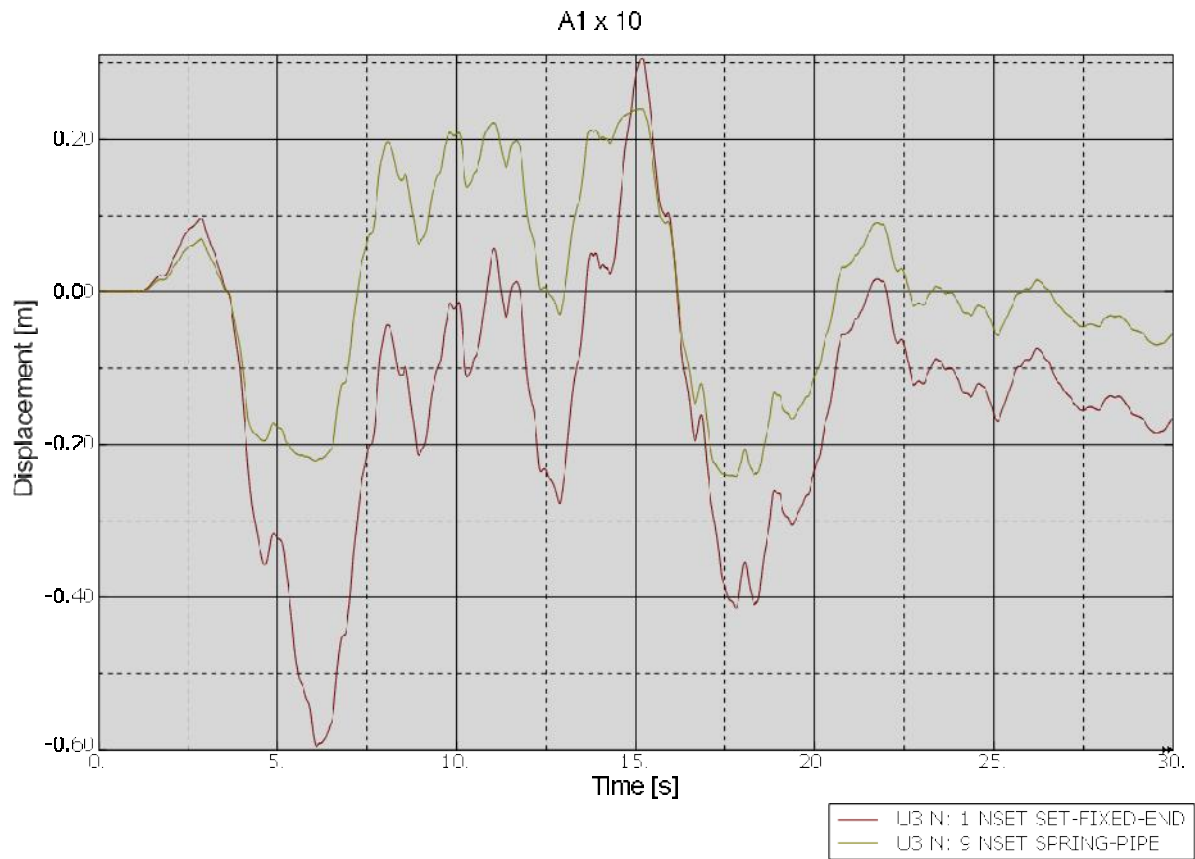


Figure 51. Displacement of the pipe in global 3 direction in the fixed end and at the spring (A1x10).

7 Conclusions and future work

Different kinds of ways to numerically model with finite element code Abaqus the pipe runs and their supports are studied. A pipe guillotine break with whipping is chosen as a dynamic analysis case. Another dynamic case is earthquake and it is preliminarily studied. Simple and typical nuclear power plant pipeline geometry and materials are chosen. The chosen basic elbow element model is based on the previous studies within the same project, where it was found adequate. Some parameters and properties are improved from the previous studies. Some sensitivity studying is conducted.

The post-yield behaviour of the pipe steel material has some notable effect on the behaviour of the pipe in a guillotine pipe break. The maximum forces were of different magnitude by several percentages, but in every case with otherwise same parameter values a plastic hinge was formed at the restraint and the analysis terminated. Obviously, rate dependence makes the structure slightly stiffer dynamically. The behaviour is smoother but after some 0.1 seconds, the spring forces are of the same magnitude.

The inner pressure of the pipe and its assumed decay after the pipe break has a major influence on the results. If the pressure rapidly decays instead of being constant, the pipe still hits the restraint, but the force is less than half and no plastic hinge is formed.

By comparing the results with different types of spring behaviours and a detailed finite element modelling of the pipe and restraint, it was seen that the spring element should include the gap and some softening, i.e. curvature in the stiffness curve, but preferably not the stress-strain curve of the material directly incorporated in the stiffness of the spring.

The pipe support element ITSUNI provided by Abaqus acts in an equal way to the spring element, when the same spring behaviour is included. However, there are some uncertainties and problems in defining the initial gap between the pipe and the restraint. In a case of a single rod-like restraint, separate spring elements are more adequate, but in case of several beams, trusses or a grid, pipe support element can be more adequate.

The mass of the water has only minor effect on the dynamic behaviour of the pipe in this kind of highly dynamic loading. The maximum forces were almost the same with or without the water mass.

Earthquake simulation was briefly studied with the same model. The nonlinear dynamic analyses were conducted according to the Eurocodes. The analyses were successful and an officially approved earthquake assessment for this kind of components is possible to be made in the same manner.

References

Abaqus Manuals, 2007. Version 6.7-2. Abaqus inc.

Abaqus Manuals, 2009. Version 6.9-2. Dassault Systèmes.

Brandt, T., Lestinen, V., Toppila, T., Kähkönen, J., Timperi, A., Pättikangas, T., Karppinen, I., 2008. "Validation of fluid-structure interaction calculations in a large-break loss of coolant accident". Proceedings of the 16th International Conference on Nuclear Engineering, ICONE16, May 11-15, 2008, Orlando, Florida, USA. ASME. Orlando, Florida. Vol. 2 (2008), 245 – 254.

Calonius, K., 2008. "Preliminary Numerical Studies on Dynamic Behaviour of Pipelines". VTT Public Research Report, VTT-R-01637-08.

Calonius, K., 2009a. Numerical Studies on Dynamic Behaviour of Pipelines. VTT Research Report VTT-R-01025-09.

Calonius, K., 2009b. Numerical Studies on Dynamic Behaviour of Pipelines. 20th International Conference on Structural Mechanics in Reactor Technology (SMiRT 20-Division III, Paper 3141), Espoo, Finland, August 9-14, 2009. 11 p.

Eurocode, 2004. Eurocode 8: Design of structures for earthquake resistance - Part 1: General rules, seismic actions and rules for buildings. BS EN 1998-1:2004.

Fulop, L., 2009. E-mails and conversations with Ludovic Fulop and the artificial signal created by him.

Haar, L., Gallagher, J.S., Kell, G.S., 1984. "NBS/NRC steam tables. National Standard Reference Data System. USA."

Micheli, I., Zanaboni, P. Transactions of the SMiRT Conference, 2003. Paper #J05-4. "An Analytical Validation of Simplified Methods for the Assessment of Pipe Whip characteristics".

Robbe, M., Lepareux, M., Trollat, C., 1999. Transactions of the SMiRT-15 Conference, 1999. Paper #J05-4. "Hydrodynamic Loads on a PWR Primary Circuit due to a LOCA-Pipe Computations with the CASTEM-PLEXUS Code".

Vörös, G., Zsidi, Z., 2002. "Analysis of the effects of postulated pipe rupture". Gépezet 2002, Budapest. 307-310.